weeks. Local application of siRNA/ATCOL complex was shown to be effective to target the vascular endothelial growth factor gene in a xenografted tumor,[18] while ATCOL was used for systemic siRNA delivery into tumor-bearing mouse models and proved to be effective for silencing exogenous genes as luciferase and metastasis-associated genes as EZH2.[6] However, it has not been elucidated until this study whether the siRNA complex could have an effect of muscle growth on normal tissues by repression of muscle-specific genes. It has been thought that the enhanced permeability and retention (EPR) effect in tumor tissues could facilitate selective targeting of siRNA/polymer complex.[6] In spite of the significance of the EPR effect in tumor therapies, it is noticeable that normal and nontumor diseased tissues can be targets for siRNA-based drugs applied systemically. It was reported that nuclease activity to siRNA could be prevented[18] and cellular uptake of siRNAs was elevated by ATCOL.[5] Although the precise mechanisms by which ATCOL achieves these effects have not been elucidated to date, ATCOL complexed with DNA molecules was demonstrated to be efficiently transduced into mammalian cells.[19] Thus, similarly siRNA/ATCOL complexes may be transduced into cells probably by the same mechanisms as observed for DNA molecules. As a simple administration of myostatin-siRNA/ATCOL complex has a muscle growth effect, this novel method for fighting against muscle atrophy would be of considerable value for clinical applications. In tumor-bearing mice, it was reported that ATCOL could distribute siRNAs against luciferase to normal liver, lung, spleen and kidney tissues as well as bone-metastatic lesions.[6] ATCOL was also reported to display low toxicity and low immunogenicity when it is transplanted *in vivo*.[20,21] Taken together with our results, application of siRNAs with ATCOL would be promising for a therapeutic remedy against various diseases not only of muscles, but also of these organs.

Acknowledgements

We thank Drs Shin-ichiro Nishimatsu, Tsutomu Nohno, Department of Molecular Biology, Kawasaki Medical School for valuable advice. We also thank Shizuka Sasano, Division of Neurology, Kawasaki Medical School and Megumu Kita, Laboratory Animal Center, Kawasaki Medical School for their technical assistances. This work was supported by a Research Grant (14B-4) for Nervous and Mental Disorders from the Ministry of Health, Labour and Welfare; a Grant (15131301) for Research on Psychiatric and Neurological Diseases and Mental Health from the Ministry of Health, Labour and Welfare of Japan and from JSPS KAKENHI (14370212) to SN, YO and YS and by Research Project Grants (15-115B and 16-601) from Kawasaki Medical School to YO and YS.

References

1 Fire A, Xu S, Montgomery MK, Kostas SA, Driver SE, Mello CC. Potent and specific genetic interference by double-stranded RNA in *Caenorhabditis elegans*. *Nature* 1998; **391**: 806–811.

2 Elbashir SM, Harborth J, Lendeckel W, Yalcin A, Weber K, Tuschl T. Duplexes of 21-nucleotide RNAs mediate RNA interference in cultured mammalian cells. *Nature* 2001; **411**: 494–498.

3 de Fougerolles A, Vornlocher HP, Maraganore J, Lieberman J. Interfering with disease: a progress report on siRNA-based therapeutics. *Nat Rev Drug Discov* 2007; **6**: 443–453.

4 Gary DJ, Puri N, Won YY. Polymer-based siRNA delivery: perspectives on the fundamental and phenomenological distinctions from polymer-based DNA delivery. *J Control Release* 2007; **121**: 64–73.

5 Minakuchi Y, Takeshita F, Kosaka N, Sasaki H, Yamamoto Y, Kouno M *et al*. Atelocollagen-mediated synthetic small interfering RNA delivery for effective gene silencing *in vitro* and *in vivo*. *Nucleic Acids Res* 2004; **32**: e109.

6 Takeshita F, Minakuchi Y, Nagahara S, Honma K, Sasaki H, Hirai K *et al*. Efficient delivery of small interfering RNA to bone-metastatic tumors by using atelocollagen *in vivo*. *Proc Natl Acad Sci USA* 2005; **102**: 12177–12182.

7 Takeshita F, Ochiya T. Therapeutic potential of RNA interference against cancer. *Cancer Sci* 2006; **97**: 689–696.

8 McPherron AC, Lawler AM, Lee SJ. Regulation of skeletal muscle mass in mice by a new TGF-beta superfamily member. *Nature* 1997; **387**: 83–90.

9 Deconinck N, Dan B. Pathophysiology of Duchenne muscular dystrophy: current hypotheses. *Pediatr Neurol* 2007; **36**: 1–7.

10 Foster K, Foster H, Dickson JG. Gene therapy progress and prospects: Duchenne muscular dystrophy. *Gene Therapy* 2006; **13**: 1677–1685.

11 Bogdanovich S, Krag TO, Barton ER, Morris LD, Whittemore LA, Ahima RS *et al*. Functional improvement of dystrophic muscle by myostatin blockade. *Nature* 2002; **420**: 418–421.

12 Nishi M, Yasue A, Nishimatsu S, Nohno T, Yamaoka T, Itakura M *et al*. A missense mutant myostatin causes hyperplasia without hypertrophy in the mouse muscle. *Biochem Biophys Res Commun* 2002; **293**: 247–251.

13 Ohsawa Y, Hagiwara H, Nakatani M, Yasue A, Moriyama K, Murakami T *et al*. Muscular atrophy of caveolin-3-deficient mice is rescued by myostatin inhibition. *J Clin Invest* 2006; **116**: 2924–2934.

14 Magee TR, Artaza JN, Ferrini MG, Vernet D, Zuniga FI, Cantini L *et al*. Myostatin short interfering hairpin RNA gene transfer increases skeletal muscle mass. *J Gene Med* 2006; **8**: 1171–1181.

15 Artaza JN, Bhasin S, Magee TR, Reisz-Porszasz S, Shen R, Groome NP *et al*. Myostatin inhibits myogenesis and promotes adipogenesis in C3H 10T(1/2) mesenchymal multipotent cells. *Endocrinology* 2005; **146**: 3547–3557.

16 Bulfield G, Siller WG, Wight PA, Moore KJ. X chromosome-linked muscular dystrophy (mdx) in the mouse. *Proc Natl Acad Sci USA* 1984; **81**: 1189–1192.

17 McPherron AC, Lee SJ. Suppression of body fat accumulation in myostatin-deficient mice. *J Clin Invest* 2002; **109**: 595–601.

18 Takei Y, Kadomatsu K, Yuzawa Y, Matsuo S, Muramatsu T. A small interfering RNA targeting vascular endothelial growth factor as cancer therapeutics. *Cancer Res* 2004; **64**: 3365–3370.

19 Honma K, Ochiya T, Nagahara S, Sano A, Yamamoto H, Hirai K *et al*. Atelocollagen-based gene transfer in cells allows high-throughput screening of gene functions. *Biochem Biophys Res Commun* 2001; **289**: 1075–1081.

20 Ochiya T, Nagahara S, Sano A, Itoh H, Terada M. Biomaterials for gene delivery: atelocollagen-mediated controlled release of molecular medicines. *Curr Gene Ther* 2001; **1**: 31–52.

21 Sano A, Maeda M, Nagahara S, Ochiya T, Honma K, Itoh H *et al*. Atelocollagen for protein and gene delivery. *Adv Drug Deliv Rev* 2003; **55**: 1651–1677.

Supplementary Information accompanies the paper on Gene Therapy website (http://www.nature.com/gt)

ARTHRITIS & RHEUMATISM
Vol. 58, No. 2, February 2008, pp 389–400
DOI 10.1002/art.23163

Effective Treatment With Oral Administration of Rebamipide in a Mouse Model of Sjögren's Syndrome

Masayuki Kohashi,[1] Naozumi Ishimaru,[2] Rieko Arakaki,[2] and Yoshio Hayashi[2]

Objective. **To determine whether oral administration of rebamipide, a mucosal protective agent, is effective in the treatment of Sjögren's syndrome (SS) in the NFS/*sld* mouse model of the disease.**

Methods. **NFS/*sld* mice were given daily oral doses of rebamipide (0.3 mg/kg of body weight or 3 mg/kg) or vehicle alone starting from the age of 4 weeks to the age of 8 weeks. The volume of saliva and tears was monitored during and after treatment. After the final dose, histologic features of the tissues, TUNEL+ apoptotic duct cells in affected glands, T cell and cytokine function, and levels of immunoglobulin isotypes and serum autoantibodies were examined.**

Results. **The 3-mg/kg dose of rebamipide prevented the development of autoimmune lesions. The average volume of saliva in rebamipide-treated mice was significantly higher than that in control mice. We found decreased TUNEL+ apoptotic duct cells in the salivary and lacrimal glands of rebamipide-treated mice as compared with control mice. Rebamipide treatment suppressed the activation of CD4+ T cells and Th1 cytokines (interleukin-2, interferon-γ) associated with impaired NF-κB activity. Production of serum autoantibodies, IgM, and IgG1 was clearly inhibited.**

Conclusion. **Our findings demonstrate the efficacy of oral administration of rebamipide in the treatment of SS. Rebamipide represents a new therapeutic strategy for the treatment of patients with sicca symptoms caused by SS, as well as for patients with other diseases.**

Sjögren's syndrome (SS) is an autoimmune disorder characterized by lymphocytic infiltrates and destruction of the salivary and lacrimal glands, as well as systemic production of autoantibodies to the RNP particles SSA/Ro and SSB/La (1–3). Although the specificity of cytotoxic T lymphocyte function has been an important issue in studies of organ-specific autoimmune responses, the mechanisms responsible for tissue destruction in SS remain to be fully elucidated. The immune system has acquired regulatory mechanisms that preclude the reactivity of mature T cells to self antigens presented by major histocompatibility complex (MHC) molecules, while maintaining an ability to respond to non-self antigens presented by self MHC molecules (4,5). The dysregulation of T cell tolerance is considered to be responsible for many types of autoimmune diseases, and a variety of mechanisms involved in the initiation of autoimmune diseases have been proposed (6–10).

Data from our previous studies demonstrated that autoreactive CD4+ T cells play a pivotal role in the development of autoimmune exocrinopathy in the NFS/*sld* mouse model of SS (11). It is now evident that the interaction of Fas with FasL regulates a large number of pathophysiologic processes of apoptosis, including autoimmune diseases (11,12). Previous studies have also confirmed the observation that apoptotic cells in various cell types are implicated as the source of autoantigen when stimulated with different proapoptotic stimuli (13).

On the other hand, natural autoantibody appears to be primarily IgM polyreactive antibody of low affinity, which is quite different from the monospecific high-affinity IgG antibody usually associated with autoimmune disease (14). It is important to note that au-

Supported in part by the Ministry of Education, Science, Sports, and Culture of Japan (Grants-in-Aid for Scientific Research 17109016 and 17689049) and the Uehara Memorial Foundation.

[1]Masayuki Kohashi, PhD: University of Tokushima Graduate School, and Otsuka Pharmaceutical Company, Ltd., Tokushima, Japan; [2]Naozumi Ishimaru, DDS, PhD, Rieko Arakaki, PhD, Yoshio Hayashi, DDS, PhD: University of Tokushima Graduate School, Tokushima, Japan.

Address correspondence and reprint requests to Yoshio Hayashi, DDS, PhD, Department of Oral Molecular Pathology, Institute of Health Biosciences, University of Tokushima Graduate School, 3 Kuramoto-cho, Tokushima 770-8504, Japan. E-mail: hayashi@dent.tokushima-u.ac.jp.

Submitted for publication June 15, 2007; accepted in revised form October 26, 2007.

toantigens released from the intracytoplasmic environment will not, under normal conditions, stimulate the production of pathogenic IgG autoantibodies capable of causing tissue damage (14,15). During an autoimmune disease, levels of IgM autoantibodies are high (16) due to the stimulation of IgM autoantibody–producing cell lines by the release of autoantigens from target cells. IgG antibodies are the primary mediators of protective humoral immunity against pathogens, but they can also be pathogenic. Acting as cytotoxic molecules or as immune complexes, IgG autoantibodies are the principal mediators of autoimmune diseases such as idiopathic thrombocytopenia, autoimmune hemolytic anemia, and systemic lupus erythematosus, and may contribute to other autoimmune diseases, such as rheumatoid arthritis, type 1 diabetes mellitus, and multiple sclerosis (17).

Rebamipide (2-[4-chlorobenzoylamino]-3-[2(1*H*)quinolinon-4-yl]propionic acid; OPC-12759) is a mucosal protective agent used for the treatment of gastritis and gastric ulcer. It has recently been reported that rebamipide works as an antiinflammatory agent in both acute and chronic inflammation and has an inhibitory effect on proinflammatory cytokines (18). Experimental data have shown that rebamipide can prevent Dextran sulfate sodium–induced colitis in rats (19). A recent study demonstrated the protective effect of rebamipide on the intestinal barrier, namely, its ability to reinforce the epithelial barrier capacity and to decrease macromolecular transport across this barrier (20). At the same time, the study demonstrated the immunoregulatory properties of rebamipide, which is capable of regulating lymphocyte proliferation and cytokine secretion (20).

The aim of the present study was to investigate the effects of oral administration of rebamipide on various parameters of autoimmune responses and on serum levels of autoantibodies, immunoglobulins, and inflammatory cytokines in a murine model of SS. We hypothesized that in this model of SS, the immunomodulatory activity of rebamipide against autoimmune responses to tissue-specific autoantigens would be a good therapeutic approach.

MATERIALS AND METHODS

Mice and experimental design. Female mice of the NFS/N strain carrying the mutant gene *sld* (21) were reared in our specific pathogen–free mouse colony and given food and water ad libitum. Thymectomy was performed on day 3 after birth in the NFS/*sld* mice (22). A total of 35 NFS/*sld* mice that had been subjected to thymectomy on day 3 after birth were investigated in the present study. An additional group of 10 mice not subjected to thymectomy were also investigated. Rebamipide (Otsuka Pharmaceutical, Tokushima, Japan) was prepared as a suspension in 0.5% carboxymethylcellulose (Dai-Ichi Chemical Industries, Tokyo, Japan) in water.

The following experimental groups were studied: a vehicle-treated control group, which received oral administration of vehicle alone (n = 12), and 2 rebamipide-treated groups, which received oral administration of rebamipide at a dose of either 0.3 mg/kg of body weight (n = 12) or 3 mg/kg of body weight (n = 11). Thymectomized NFS/*sld* mice were given daily oral treatment with rebamipide or vehicle, starting from the age of 4 weeks to age 8 weeks. Nonthymectomized mice (n = 10) received oral administration of vehicle alone.

OT-2 mice (C57BL/6-Tg[TcraTcrb]452Cbn/J) were obtained from Dr. J. Sprent (Garvan Institute of Medical Research, Darlinghurst, New South Wales, Australia). These mice (n = 5) were used in the transfer experiment.

All experiments were approved by the Animal Ethics Board of the University of Tokushima.

Histologic assessment. At the end of the treatment period, all organs were removed from the mice, fixed in 4% phosphate buffered formaldehyde (pH 7.2), and prepared for histologic examination. Formalin-fixed tissue sections were stained with hematoxylin and eosin, and 3 pathologists (NI, RA, and YH) independently evaluated the histologic features without knowledge of the condition of each mouse. Histologic changes were scored on a scale of 1–3, where 1 = no change or slight lymphoid cell infiltration (slight), 2 = mild lymphoid cell infiltration (moderate), and 3 = marked lymphoid cell infiltration with tissue destruction (severe). Histologic evaluation was performed in a blinded manner, and 1 tissue section from each salivary and lacrimal gland was evaluated.

TUNEL assay. Apoptotic cells were detected in tissue sections using the in situ TUNEL kit (Wako Pure Chemical, Osaka, Japan), as previously described (23). Briefly, sections were incubated with proteinase K (400 mg/ml) for 5 minutes, and then presoaked for 10 minutes in terminal deoxynucleotidyl transferase (TdT) buffer (0.5 μmoles/liter of cacodylate, 1 mmole/liter of $CoCl_2$, 0.5 μmoles/liter of dithiothreitol, 0.05% bovine serum albumin, 0.15 moles/liter of NaCl). Sections were incubated for 2 hours at 37°C in 25 μl of TdT solution containing 1× terminal transferase buffer, 0.5 nmoles of biotin-labeled dUTP, and 10 units of TdT.

After the TdT reaction, sections were soaked in TdT blocking buffer (300 nmoles/liter of NaCl, 30 mmoles/liter of trisodium citrate-2-hydrate), incubated with horseradish peroxidase (HRP)–conjugated streptavidin for 30 minutes at room temperature, and developed for 10 minutes in phosphate buffered citrate (pH 5.8) containing 0.6 mg/ml of 3,3′-diaminobenzidine tetrahydrochloride dihydrate (DAB). Nuclei were counterstained with methyl green.

Flow cytometric analysis. Surface markers were identified with monoclonal antibodies (mAb) and using an Epics flow cytometer (Beckman Coulter, Miami, FL). Rat mAb against fluorescein isothiocyanate (FITC)–, phycoerythrin (PE)–, or PE-Cy5–conjugated anti-B220, Thy1.2, CD4, and CD8 (eBioscience, San Diego, CA) were used. For detection of T cell activation makers, FITC-conjugated anti-CD25, anti-CD44, anti-CD62L, and anti-CD69 mAb (eBioscience) were used. For detection of B cell surface IgM and IgG1, FITC-conjugated anti-IgM (eBioscience) and anti-IgG1 (BD Phar-

Mingen, San Diego, CA) mAb were used. PE-conjugated anti-Ly5.2 (eBioscience) and biotin-conjugated anti-V_β5.2 and PE-Cy5–conjugated streptavidin (both from BD PharMingen) were used for in vivo ovalbumin-specific T cell expansion. Data were analyzed with FlowJo FACS analysis software (Tree Star, Ashland, OR).

Transfer of OT-2 T cells. Purified CD4+ T cells (5×10^6) derived from the spleen of transgenic OT-2 mice were labeled with carboxyfluorescein succinimidyl ester (CFSE; Molecular Probes, Eugene, OR) and transferred intravenously into B6 (Ly5.1+) mice. One day later, ovalbumin peptide (100 μg) was injected intraperitoneally and rebamipide (0–200 μM; 250 μl per mouse) was injected intravenously into recipient mice. Three days later, cell division was evaluated by flow cytometry to detect the CFSE dilution of the Ly5.2+,V_β5.2+, CD4+ T cells.

Real-time quantitative reverse transcription–polymerase chain reaction analysis. Total RNA was extracted from cultured T cells and B cells derived from the spleen of NFS/*sld* mice with Isogen (Wako Pure Chemical), and reverse transcribed. Transcript levels of NF-κB, FasL, interferon regulatory factor 4 (IRF-4), B lymphocyte–induced maturation protein 1 (BLIMP-1), and β-actin were determined with a PTC-200 DNA Engine Cycler (MJ Research, Waltham, MA) with SYBR Premix Ex Tag (Takara, Kyoto, Japan). The following primer sequences were used: for NF-κB, 5′-ATGGCAGACGATGATCCCTA-3′ (forward) and 5′-TAGGCAAGGTCAGAATGCAC-3′ (reverse); for FasL, 5′-ACTGGACAGATATGGGCCCAC-3′ (forward) and 5′-GCCTCTGTGAGGTAGTAAGTAG-3′ (reverse); for IRF-4, 5′-GAAGCCCCAAAGCCCTCAGTCGTTG-3′ (forward) and 5′-CGCTGAGGAGGAAACTGAA-3′ (reverse); for BLIMP-1, 5′-CATTCCTGTCCCCAACGCATCAACTG-3′ (forward) and 5′-GGTGCCCAAGCACCAAAGTCATAG-3′ (reverse); and for β-actin, 5′-GTGGGCCGCTCTAGGCACCA-3′ (forward) and 5′-CGGTTGGCCTTAGGGTTCAGGGGGG-3′ (reverse). Results were calculated with DNA Engine Opicon System software (Roche Molecular Systems, Alameda, CA).

Western blot analysis. Cell extracts from the nucleus and cytoplasm of T cells and B cells were prepared using a Nuclear/Cytosol Fractionation kit (BioVision, Mountain View, CA). Cells were briefly washed, collected in ice-cold phosphate buffered saline (PBS) in the presence of phosphatase inhibitors, and centrifuged at 500 revolutions per minute for 5 minutes. The pellets were resuspended in a hypotonic buffer, treated with detergent, and centrifuged at 14,000*g* for 30 seconds. The cytoplasmic fraction was collected, the nuclei were lysed, and nuclear proteins were solubilized in lysis buffer containing protease inhibitors. A total of 10 μg of each sample per well was used for sodium dodecyl sulfate–polyacrylamide gel electrophoresis. After blocking with 5% nonfat milk, the membrane was incubated with primary antibodies against phospho-IκBα and NF-κB p65 (RelA) (Santa Cruz Biotechnology, Santa Cruz, CA). Antigen–antibody complexes were detected using a HRP-conjugated secondary antibody. Protein binding was visualized with enhanced chemiluminescence Western blotting reagent (Amersham Biosciences, Arlington Heights, IL). Anti-mouse histone H1 or GAPDH monoclonal antibody (Santa Cruz Biotechnology) was used as the control for protein loading.

Measurement of fluid secretion. Analysis of tear and saliva volumes in rebamipide-treated thymectomized NFS/*sld* mice was performed according to a previously described method (24).

Proliferation assay. CD4+ T cells (1×10^5) purified from spleen cells using anti-B220 mAb, anti-CD8 mAb, and anti-rat IgG conjugated to magnetic beads (Dynal, Oslo, Norway) were placed in RPMI 1640 containing 10% fetal calf serum (FCS), 100 units/ml of penicillin, 0.1 mg/ml of streptomycin, and 50 μM 2-mercaptoethanol and were stimulated with recombinant α-fodrin protein (JS-1) (25) or with plate-coated anti-CD3 and anti-CD28 mAb in 96-well, flat-bottomed plates for 72 hours. Then, ^{3}H-thymidine (1 μCi/well; NEN Life Science Products, Boston, MA) was pulsed into the cell mixture during the final 20 hours of culture. Incorporation of ^{3}H-thymidine was assayed with an automated liquid scintillation counter.

For detection of the proliferation of the CD4+ T cell subset, CFSE-labeled CD4+ T cells were cultured for 72 hours. The CD4+ T cells were then stained with anti-CD4 mAb, and cell division of the CD4+ gated T cells was analyzed by flow cytometer.

Assay of immunoglobulin secretion from B cells. B cells (1×10^5) purified from spleen cells using anti-CD4 mAb, anti-CD8 mAb, and anti-rat IgG conjugated to magnetic beads (Dynal) were placed in RPMI 1640 containing 10% FCS, penicillin/streptomycin, and 2-mercaptoethanol and were stimulated with 10 μg/ml of lipopolysaccharide (LPS; Sigma, St. Louis, MO) and 50 ng/ml of interleukin-4 (IL-4; eBioscience) in 96-well round-bottomed plates for 5 days. Cell surface expression of IgM and IgG1 was detected by flow cytometric analysis, and secreted IgM and IgG1 in the culture supernatants were measured by enzyme-linked immunosorbent assay (ELISA).

Serum autoantibody and cytokine ELISAs. JS-1, SSA/Ro, SSB/La, or single-stranded DNA (ssDNA) antibody was used to coat 96-well plates (24). After the plates were washed, diluted mouse sera were added. HRP-conjugated anti-mouse IgG (heavy and light chains; Vector, Burlingame, CA) was added as the secondary antibody, and *o*-phenylenediamine (OPD; Sigma) buffer was added. Antibodies were measured with an ELISA reader (Model 680; Bio-Rad, Richmond, CA) and with a spectrophotometer at 490 nm.

Serum immunoglobulins were determined by ELISA using a mouse immunoglobulin quantitation kit (Bethyl Laboratories, Montgomery, TX). Briefly, for the IgM and IgA ELISAs, sera were diluted 1:5,000 in PBS, and for the IgG ELISA, sera were diluted 1:25,000 in PBS. Plates were coated with a capture antibody and then washed with PBS–0.1% Tween 20. Diluted sera or culture supernatants were added to the plates and incubated. After washing with PBS–0.1% Tween 20, an HRP-conjugated detection antibody was added. Plates were again washed with PBS–0.1% Tween 20, and OPD buffer was added. Plates were then analyzed with a spectrophotometer at 490 nm, as described previously (26).

Levels of IL-2, interferon-γ (IFNγ), IL-4, and IL-10 in culture supernatants from splenic CD4+ T cells stimulated with anti-CD3 and anti-CD28 for 72 hours were determined by ELISA. Specific antibodies for each cytokine were used in the ELISAs, as previously described (27).

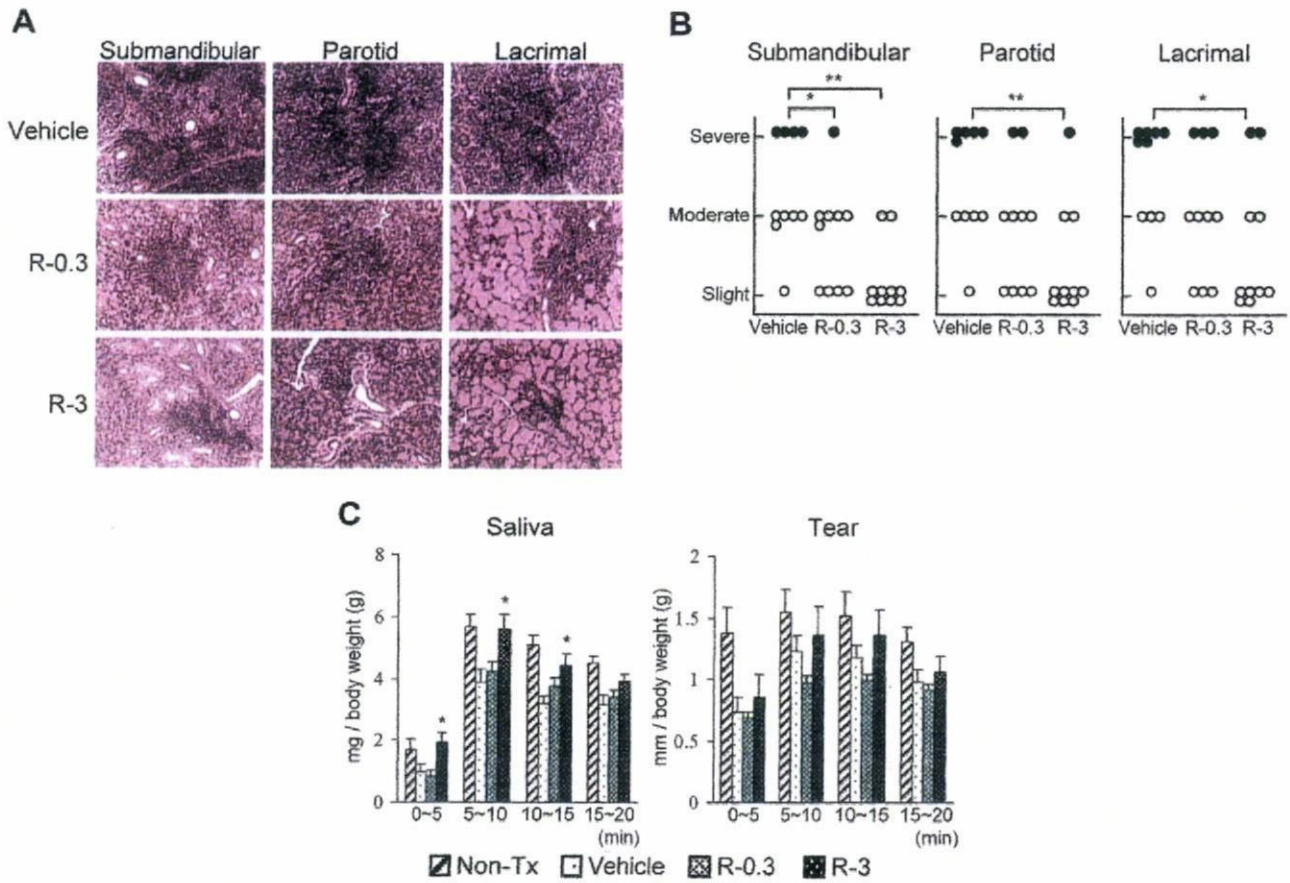

Figure 1. Therapeutic effect of rebamipide on autoimmune lesions in the NFS/*sld* mouse model of Sjögren's syndrome. Mice underwent thymectomy on day 3 after birth and were treated with vehicle, 0.3 mg/kg of rebamipide (R-0.3), or 3 mg/kg of rebamipide (R-3) from age 4 weeks to age 8 weeks. **A,** Sections of salivary and lacrimal glands from the 3 groups of mice. Results are representative of 10 mice per group (hematoxylin and eosin stained; magnification × 100). **B,** Histologic grading of inflammatory lesions in salivary and lacrimal glands from individual mice in the 3 treatment groups. * = $P < 0.05$; ** = $P < 0.01$ by lower-tailed Shirley-Williams test. The mean ± SD histology sores in the vehicle, rebamipide 0.3 mg/kg, and rebamipide 3 mg/kg groups were 2.3 ± 0.7, 1.7 ± 0.7, and 1.2 ± 0.4 for the submandibular glands, 2.4 ± 0.7, 1.8 ± 0.8, and 1.4 ± 0.7 for the parotid glands, and 2.5 ± 0.7, 2.0 ± 0.8, and 1.6 ± 0.8 for the lacrimal glands, respectively. **C,** Average saliva and tear volumes after pilocarpine administration (5 mg/kg) in mice of the 3 treatment groups and in a group of nonthymectomized (non-Tx), vehicle-treated mice at different time periods after pilocarpine administration. Values are the mean and SEM of 10–12 mice per group. * = $P < 0.05$ versus the vehicle-treated control group, by Dunnett's test.

Statistical analysis. Statistical analysis was performed using the Jonckheere trend test and the lower-tailed Shirley-Williams test, Dunnett's test, Student's *t*-test, and chi-square test, as appropriate.

RESULTS

Therapeutic effect of oral administration of rebamipide. In our previous study (22), we found that NFS/*sld* mice subjected to thymectomy on day 3 after birth began to develop autoimmune lesions of the salivary and lacrimal glands at 4 weeks of age or later, while no inflammatory lesions were observed in nonthymectomized NFS/*sld* mice. In the present study, we investigated whether oral administration of rebamipide protects NFS/*sld* mice against the development of autoimmune lesions. To evaluate whether rebamipide treatment was effective at preventing the SS autoimmune pathology, the drug or vehicle alone was administered orally each day to thymectomized NFS/*sld* mice beginning at the age of 4 weeks and continuing to the age of 8 weeks, then organs were removed for histologic analysis.

Salivary and lacrimal glands were stained with hematoxylin and eosin, and histologic features were assessed. Treatment with rebamipide at a concentration of 3 mg/kg prevented the development of autoimmune

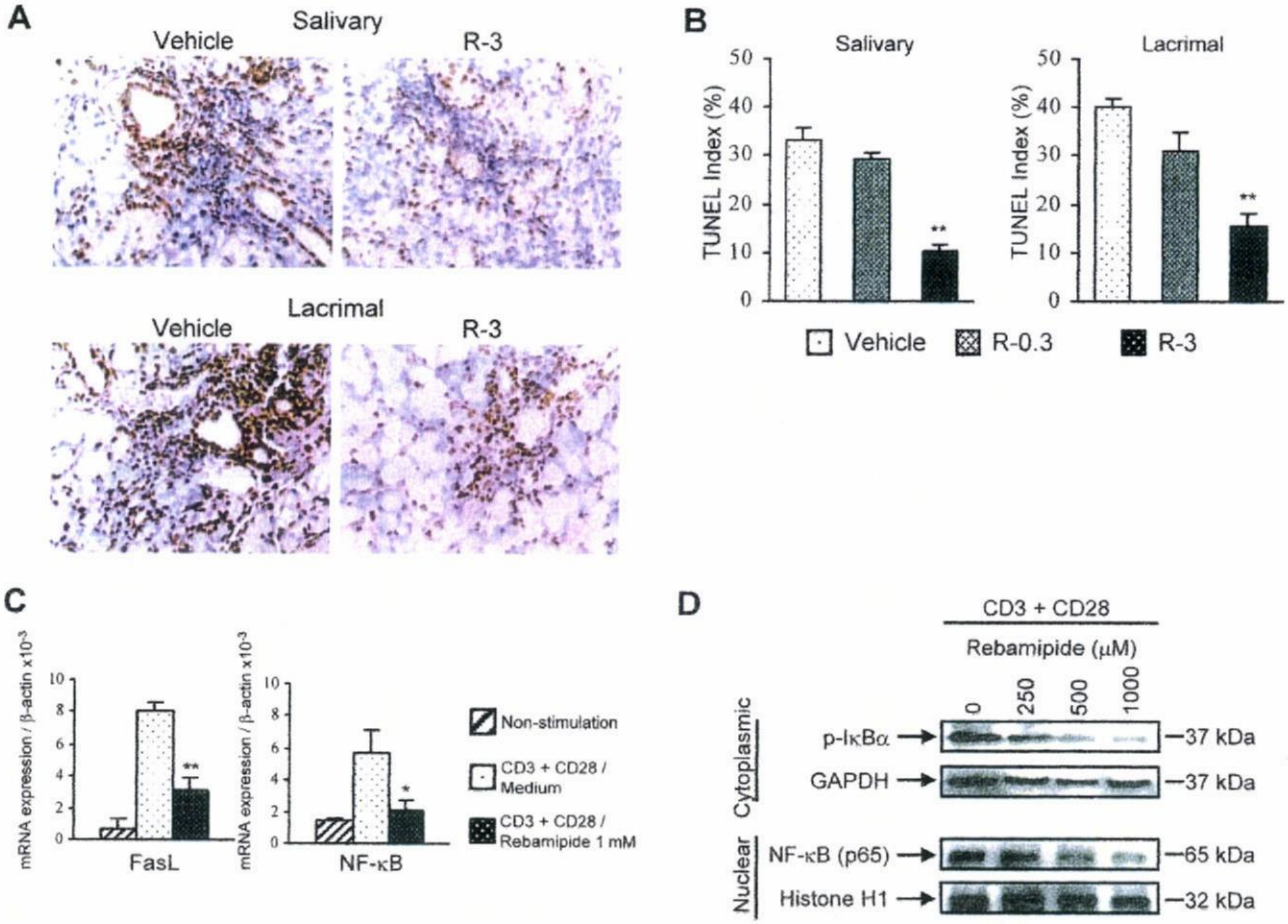

Figure 2. Inhibitory effect of rebamipide on apoptosis of salivary gland cells in the NFS/*sld* mouse model of Sjögren's syndrome. Mice underwent thymectomy on day 3 after birth and were treated with vehicle, 0.3 mg/kg of rebamipide (R-0.3), or 3 mg/kg of rebamipide (R-3) from age 4 weeks to age 8 weeks. **A,** TUNEL assay for apoptotic cells in the salivary and lacrimal glands of mice treated with vehicle or with 3 mg/kg of rebamipide. Results are representative of 5–8 mice per group (magnification × 100). **B,** Percentages of TUNEL+ salivary and lacrimal epithelial cells in the 3 treatment groups. Positive cells were enumerated using a 10 × 20–μm grid net disc covering an objective area of 0.16 mm^2 (n = 10 fields per section). Values are the mean and SEM of 5 mice per group. ** = $P < 0.01$ versus the vehicle-treated group, by Dunnett's test. **C,** Inhibitory effect of rebamipide on T cell activation. Purified CD4+ T cells derived from mouse spleens were stimulated with plate-coated anti-CD3 and anti-CD28 monoclonal antibody for 2 hours in the presence of rebamipide. Levels of mRNA for FasL and NF-κB were detected by quantitative reverse transcription–polymerase chain reaction analysis. Values are the mean and SEM expression relative to β-actin mRNA in triplicate wells. * = $P < 0.01$; ** = $P < 0.05$ versus medium containing anti-CD3 and anti-CD28, by Student's *t*-test. **D,** Phosphorylation of IκB and nuclear translocation of NF-κB in cytoplasmic and nuclear extracts of activated CD4+ T cells treated with CD3 and CD28 ligation in the presence of rebamipide, as analyzed by Western blotting. GAPDH and histone H1 were used as the respective internal controls. Results are representative of 3 independent experiments.

lesions in the submandibular ($P < 0.01$), parotid ($P < 0.01$), and lacrimal ($P < 0.05$) glands (Figures 1A and B). Rebamipide treatment at a concentration of 0.3 mg/kg prevented the development of autoimmune lesions in the submandibular glands alone ($P < 0.05$). Mononuclear cell infiltration as well as destruction of the parenchyma was inhibited in the salivary and lacrimal glands of thymectomized NFS/*sld* mice treated with rebamipide. The average saliva volume, but not tear volume, in the rebamipide-treated group was significantly higher than that in the vehicle-treated control group (Figure 1C).

We previously demonstrated that epithelial cell apoptosis via the Fas/FasL system plays an important role in the development of autoimmune lesions in this mouse model of SS, and a significant increase in TUNEL+ apoptotic epithelial duct cells in the salivary glands was detected in this mouse model (11). In the

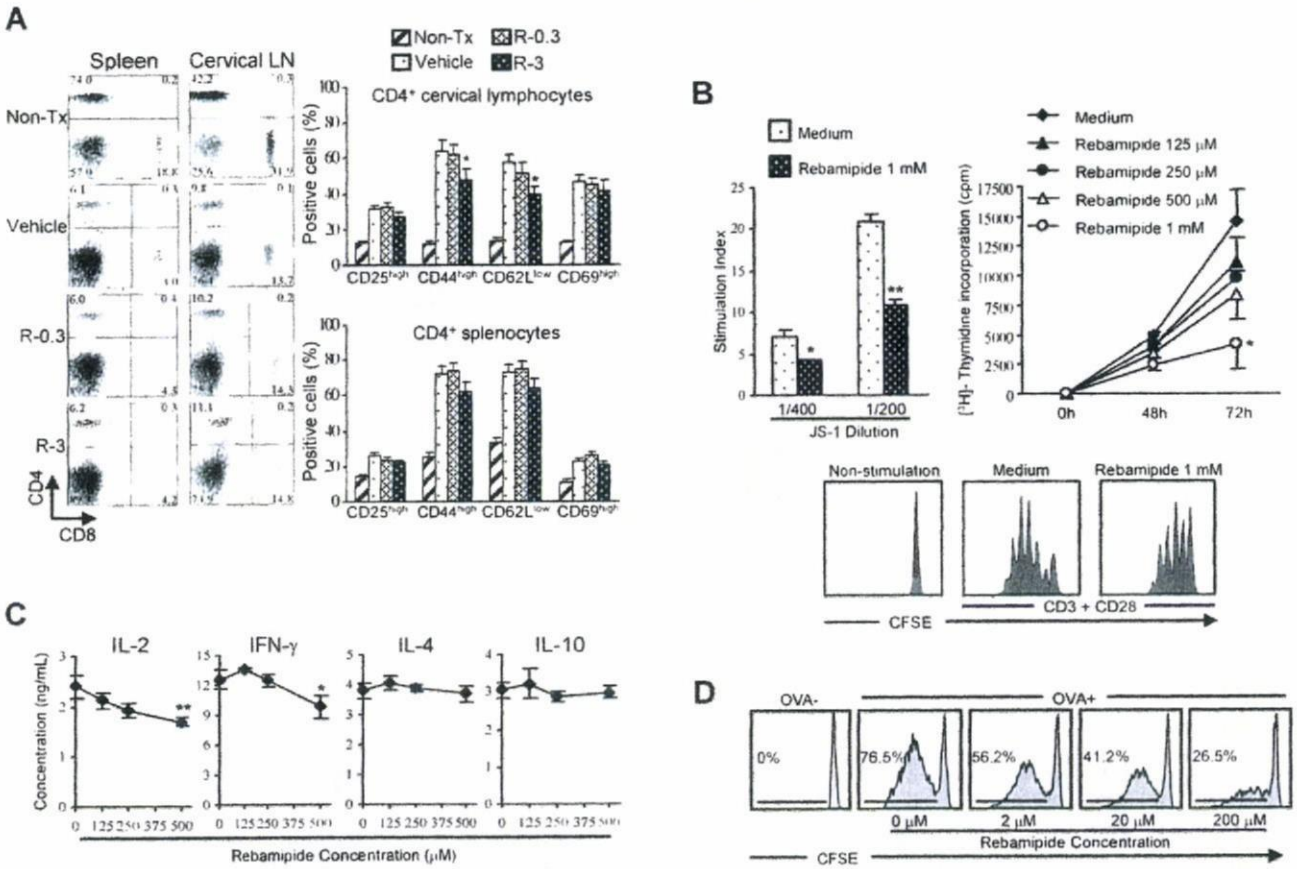

Figure 3. Effect of rebamipide on T cell phenotypes and functions in the NFS/*sld* mouse model of Sjögren's syndrome. Mice underwent thymectomy on day 3 after birth and were treated with vehicle, 0.3 mg/kg of rebamipide (R-0.3), or 3 mg/kg of rebamipide (R-3) from age 4 weeks to age 8 weeks. A group of nonthymectomized (non-Tx), vehicle-treated mice was also studied. **A,** CD4+ and CD8+ T cell subsets in the spleen and cervical lymph nodes of the 4 groups of mice, as analyzed by flow cytometry (left). Numbers shown in each compartment are the percentage of positive cells. Results are representative of 10 mice per group. Memory markers on CD4+ T cells derived from the cervical lymph nodes and spleen of the 4 groups of mice were also analyzed by flow cytometry (right). Values are the mean and SEM of 10 mice per group. **B,** Antigen-specific and nonspecific T cell responses. Purified CD4+ T cells from the spleen of thymectomized mice were cultured for 72 hours with irradiated T cell–depleted splenocytes in the presence of recombinant α-fodrin (JS-1), with and without rebamipide (top left). Values are the mean and SEM. * = $P < 0.05$; ** = $P < 0.01$ versus medium alone, by Dunnett's test. Incorporation of ^{3}H-thymidine into purified CD4+ T cells stimulated with anti-CD3 and anti-CD28 monoclonal antibodies (mAb) and treated for 48 or 72 hours with the indicated concentrations of rebamipide or medium alone was determined during the last 12 hours of culture (top right). Results are representative of 3 independent experiments. Values are the mean and SEM of triplicate wells. In addition, CD4+ T cells were labeled with carboxyfluorescein succinimidyl ester (CFSE) and were left unstimulated or were stimulated with anti-CD3 and anti-CD28 mAb for 72 hours in the presence of medium alone or 1 m*M* rebamipide (bottom). Cell division was analyzed by flow cytometry. * = $P < 0.01$ versus medium alone, by Dunnett's test. **C,** Production of interleukin-2 (IL-2), interferon-γ (IFNγ), IL-4, and IL-10 by CD4+ T cells stimulated for 72 hours with anti-CD3 and anti-CD28 mAb in the presence of medium alone or the indicated concentrations of rebamipide, as determined by enzyme-linked immunosorbent assay of culture supernatants. Results are representative of 3 independent experiments. Values are the mean ± SEM of triplicate samples. * = $P < 0.05$; ** = $P < 0.01$ versus medium alone, by Dunnett's test. **D,** Flow cytometry of CFSE-labeled CD4+ T cells (5×10^6) derived from transgenic OT-2 mice and transferred intravenously into B6 (Ly5.1+) mice. Ovalbumin (OVA) peptide (100 μg) was injected intraperitoneally, and rebamipide (0–200 μ*M*) was injected intravenously, into recipient mice. After 3 days, the CFSE dilution of Ly5.2+,V_β5.2+,CD4+ T cells was analyzed. Results are representative of 3–5 mice per group.

present study, we observed a decrease in TUNEL+ apoptotic epithelial cells in the salivary glands of mice treated with rebamipide as compared with those in vehicle-treated mice (Figures 2A and B). Indeed, expression of FasL and NF-κB genes on CD4+ T cells was significantly inhibited by rebamipide treatment (Figure 2C), possibly being consistent with the finding of decreased TUNEL+ epithelial cell apoptosis in the

Table 1. Autoantibody production in the NFS/*sld* mouse model of Sjögren's syndrome after treatment with rebamipide or vehicle alone*

Antibody	No. (%) of nonthymectomized, vehicle-treated mice (n = 10)	Treatment in thymectomized mice		
		No. (%) receiving vehicle (n = 12)	No. (%) receiving 0.3 mg/kg of rebamipide (n = 12)	No. (%) receiving 3 mg/kg of rebamipide (n = 11)
SSA/Ro	0 (0)	12 (100)	11 (92)	8 (73)†
SSB/La	0 (0)	11 (92)	10 (83)	6 (55)†
JS-1	0 (0)	7 (58)	4 (33)	4 (36)
ssDNA	0 (0)	11 (92)	12 (100)	7 (64)

* Mice were subjected to thymectomy on day 3 after birth. Autoantibodies were detected by enzyme-linked immunosorbent assay of sera obtained at the end of treatment (8 weeks of age). A positive result was defined as a value higher than the mean ± 3SD of the optical density value in nonthymectomized NFS/*sld* mice. JS-1 is an α-fodrin–specific antibody. ssDNA = single-stranded DNA.
† $P < 0.05$ versus vehicle-treated mice, by chi-square test.

rebamipide-treated mice. In addition, we confirmed the dose-dependent decrease in phosphorylation of IκB in CD4+ T cells from mice treated with rebamipide as compared with vehicle-treated controls (Figure 2D). Furthermore, nuclear translocation of NF-κB subunits (RelA and p65) in CD4+ T cells from rebamipide-treated mice had decreased remarkably compared with that in cells from vehicle-treated controls (Figure 2D).

Inhibitory effects of rebamipide on T cell activation. We next examined whether the therapeutic effect of oral administration of rebamipide on thymectomized NFS/*sld* mice was attributable to the inhibition of T cell activation. Cervical lymph node cells and spleen cells were purified from thymectomized NFS/*sld* mice treated with rebamipide or vehicle from ages 4 weeks to 8 weeks. In rebamipide-treated mice, the number of CD4+ and CD8+ T cells from the lymph node and spleen did not change with oral administration of rebamipide at either dose (Figure 3A).

We next examined CD25, CD44, CD62L, and CD69 expression on CD4+ T cells because these makers are known to be highly expressed on activated T cells and memory T cells (28). We found a decreased expression of CD4+,$CD62L^{low}$ effector T cells in lymph nodes from mice treated with rebamipide, as compared with those from the control group (Figure 3A). In contrast, the expression of these markers on splenic CD4+ T cells from rebamipide-treated mice was similar to that in splenic CD4+ T cells from vehicle-treated controls (Figure 3A). It has recently been demonstrated that autoimmunity could be induced by specific in vivo expansion of CD4+,$CD62L^{low}$ effector T cells (29).

Inhibitory effects of rebamipide on T cell proliferation and cytokine production. We previously reported that CD4+ T cells from thymectomized mice responded to the α-fodrin peptide JS-1 (25). Thus, we examined whether the rebamipide treatment affects the JS-1–specific proliferative response of splenic CD4+ T cells. A significant decrease in autoantigen (JS-1)–specific T cell proliferation was observed in CD4+ T cells treated with rebamipide (Figure 3B, top left). These results suggest that rebamipide treatment reduced the expansion of JS-1–specific T cells in mice, which is consistent with the low levels of CD4+,$CD62L^{low}$ effector T cells in the rebamipide-treated mice. The proliferative response of anti-CD3 and anti-CD28 mAb-stimulated CD4+ T cells was also decreased by the addition of rebamipide in a dose-dependent manner (Figure 3B, top right). Furthermore, when CFSE-labeled CD4+ T cells were stimulated with anti-CD3 and anti-CD28 mAb in the presence of rebamipide for 72 hours, cell division was suppressed by rebamipide (Figure 3B, bottom).

To confirm the inhibitory effect of rebamipide, an in vitro cytokine assay was performed using splenic CD4+ T cells stimulated with anti-CD3 and anti-CD28. We obtained clear evidence that rebamipide treatment inhibited the production of Th1 (IL-2 and IFNγ), but not Th2 (IL-4 and IL-10), cytokines (Figure 3C). In serum samples, we detected no IL-2, IL-4, or IFNγ in mice treated with rebamipide (data not shown).

It was still unclear whether the antigen-specific T cell response in a normal mouse strain is inhibited by rebamipide. Therefore, CFSE-labeled T cells from OT-2 mice transgenic for ovalbumin-specific T cell receptor

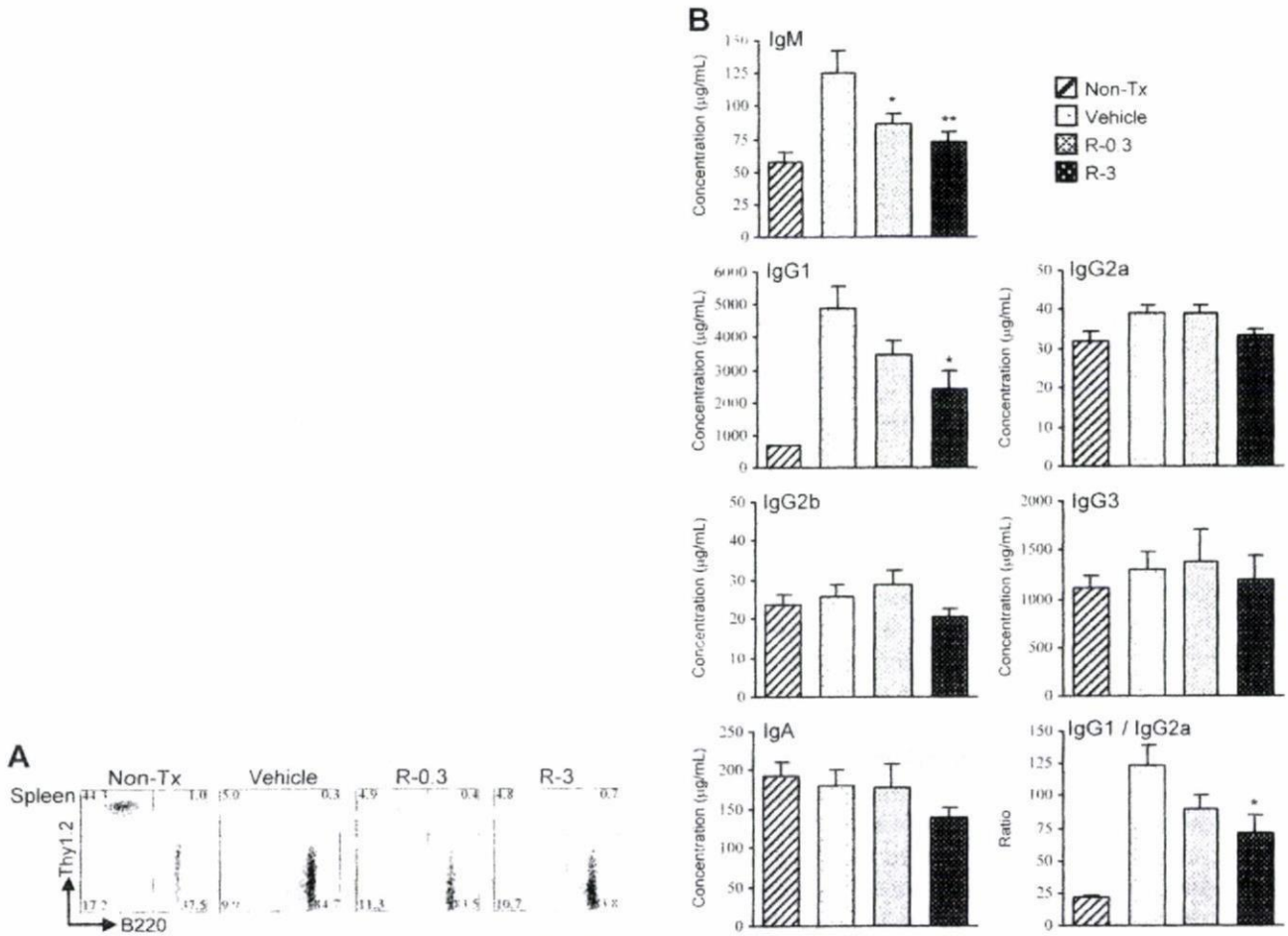

Figure 4. Effect of rebamipide on B cell function in the NFS/*sld* mouse model of Sjögren's syndrome after treatment with rebamipide. Mice underwent thymectomy on day 3 after birth and were treated with vehicle, 0.3 mg/kg of rebamipide (R-0.3), or 3 mg/kg of rebamipide (R-3) from age 4 weeks to age 8 weeks. A group of nonthymectomized (non-Tx), vehicle-treated mice was also studied. **A,** Thy1.2+ and B220+ cell subsets in the spleen of the 4 groups of mice, as determined by flow cytometry. Numbers shown in each compartment are the percentage of positive cells. Results are representative of 10–12 mice per group. **B,** Serum concentrations of immunoglobulin subclasses in the 4 groups of mice, as determined by enzyme-linked immunosorbent assay. Values are the mean and SEM of 10 mice per group. * = $P < 0.05$; ** = $P < 0.01$ versus the vehicle-treated group, by Dunnett's test.

were transferred into B6 (Ly5.1+) mice, and ovalbumin peptide was injected into the mice together with rebamipide. Treatment with rebamipide resulted in a dose-dependent inhibition of ovalbumin-specific T cell expansion in vivo (Figure 3D).

Reduced serum autoantibody production with rebamipide treatment. Sera were collected after rebamipide and vehicle treatment to evaluate the production of autoantibodies. Thymectomized NFS/*sld* mice have high titers of serum autoantibody against recombinant α-fodrin protein (JS-1) (25). We examined whether oral administration of rebamipide affected serum levels of autoantibody against α-fodrin in this mouse model of SS. As shown in Table 1, the titer of autoantibody against α-fodrin (JS-1) was considerably lower in mice treated with rebamipide than in mice treated with vehicle. The decreased serum titer of autoantibody against α-fodrin suggests that oral administration of rebamipide affected the autoimmune pathology and was able to suppress the systemic production of α-fodrin–specific autoantibody. We also examined serum titers of autoantibodies that are often associated with SS: anti-SSA/Ro, anti-SSB/La, anti-ssDNA, and anti–α-fodrin (30–33). Serum titers of anti-SSA/Ro and anti-SSB/La autoantibodies were significantly decreased in mice treated with rebamipide, but titers of anti–α-fodrin were not statistically significantly different from those in the control mice (Table 1).

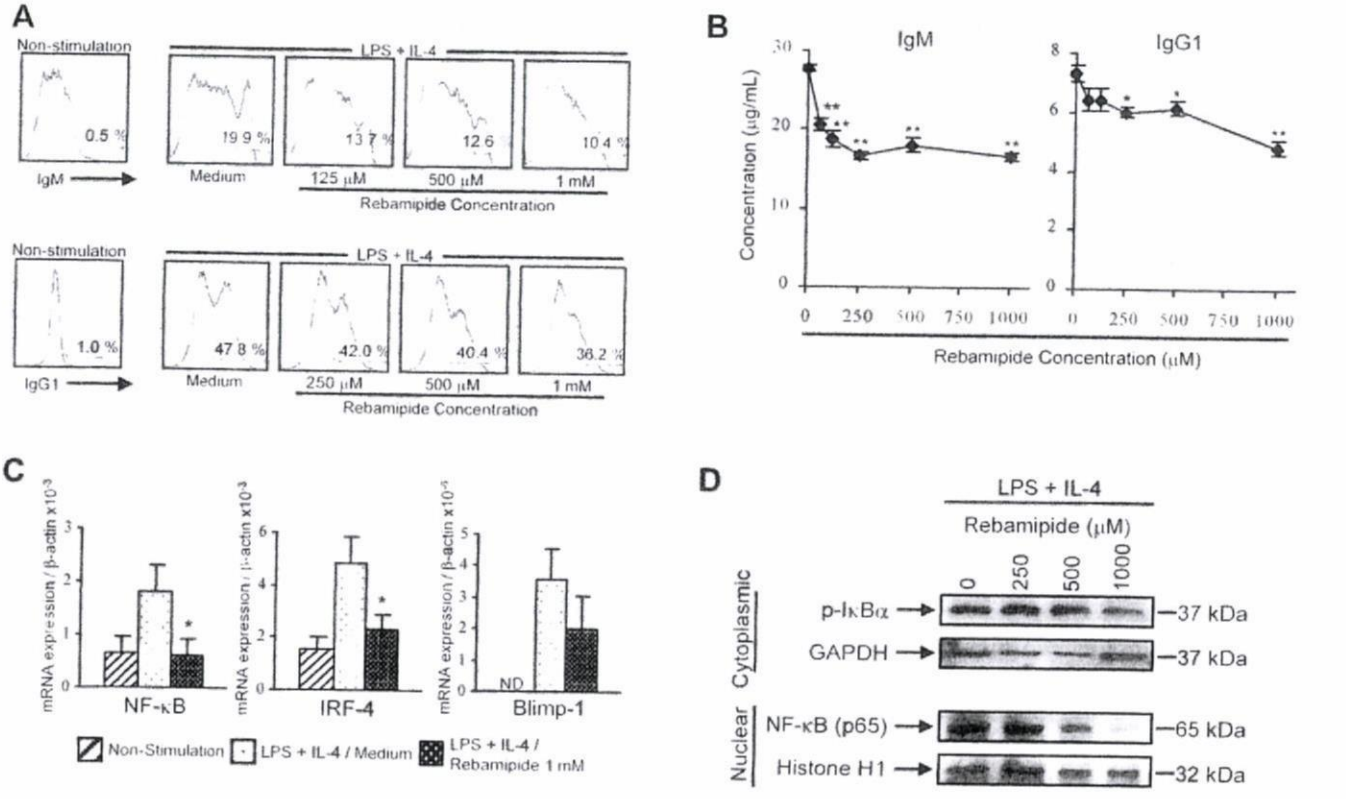

Figure 5. Effect of rebamipide on immunoglobulin production in the NFS/*sld* mouse model of Sjögren's syndrome. Mice underwent thymectomy on day 3 after birth and were treated with 3 mg/kg of rebamipide from age 4 weeks to age 8 weeks. **A,** Cell surface expression of IgM and IgG1, as detected by flow cytometry. Enriched splenic B cells were left unstimulated or were stimulated with lipopolysaccharide (LPS) and interleukin-4 (IL-4) in the presence of the indicated concentrations of rebamipide for 5 days. Values are the percentage of positive cells. **B,** Secretion of IgM and IgG1 into supernatants from B cells stimulated for 5 days with LPS and IL-4 in the presence of the indicated concentrations of rebamipide, as detected by enzyme-linked immunosorbent assay. Values are the mean ± SEM of 10 mice. * = $P < 0.05$; ** = $P < 0.01$ versus medium alone, by Dunnett's test. **C,** Expression of mRNA for NF-κB, interferon regulatory factor 4 (IRF-4), and B lymphocyte–induced maturation protein 1 (BLIMP-1), by stimulated B cells, as determined by quantitative reverse transcription–polymerase chain reaction analysis. Results are representative of 3 independent experiments. Values are the mean and SEM expression relative to β-actin mRNA in triplicate wells. * = $P < 0.05$ versus medium alone, by Student's *t*-test. ND = not detected. **D,** Phosphorylation of IκB and nuclear translocation of NF-κB in cytoplasmic and nuclear extracts of activated B cells treated with LPS and IL-4 in the presence of rebamipide, as analyzed by Western blotting. GAPDH and histone H1 were use as the respective internal controls. Results are representative of 3 independent experiments.

Reduced serum immunoglobulin levels with rebamipide treatment. In rebamipide-treated mice, the number of splenic B220+ B cells did not change with oral administration of either dose of rebamipide (Figure 4A). We found that thymectomized NFS/*sld* mice developed hypergammaglobulinemia involving both IgG1 and IgM as compared with nonthymectomized control mice (Figure 4B). Rebamipide-treated mice showed prominent inhibition of serum IgM and IgG1 levels ($P < 0.01$), but not the other IgG subclasses or IgA (Figure 4B). This may indicate that oral administration of rebamipide affected all B cell function, which was able to suppress systemic secretion of IgM and IgG1.

Inhibitory effects of rebamipide on immunoglobulin secretion. To confirm the inhibitory effects of rebamipide on IgM and IgG1 secretion, we examined the effects of in vitro treatment with rebamipide using splenic B220+ B cells stimulated with LPS and IL-4. We found that rebamipide inhibited B cell production of IgM and IgG1, as determined by flow cytometry (Figure 5A). Rebamipide also inhibited IgM and IgG1 in culture supernatants, as determined by ELISA (Figure 5B). Both of these effects were dose-dependent. Since rebamipide treatment in this mouse model of SS inhibited the production of autoantibodies and immunoglobulins, we also examined the transcriptional activity of NF-κB,

IRF-4, and BLIMP-1. Significant inhibitory effects of rebamipide on the expression of mRNA for NF-κB and IRF-4, transcription factors that are associated with B cell activation and differentiation, were observed (Figure 5C). We confirmed the dose-dependent decrease in phospho-IκB and NF-κB subunits (p65) in activated B cells stimulated with LPS and IL-4 as compared with vehicle-treated controls (Figure 5D).

DISCUSSION

Since studies of animal models of autoimmune disorders should eventually give rise to appropriate potential treatments in humans with those diseases, it is important to identify the best therapeutic approach by which cells of the immune system can be specifically affected without causing side effects. In this regard, antigen-specific down-regulation of autoimmune processes is considered to be the most suitable therapy (34–36). The findings of the present study of rebamipide treatment in the NFS/*sld* mouse model of Sjögren's syndrome confirm the protective effect of rebamipide on the functional recovery of T cells and B cells in this autoimmune exocrinopathy, probably based on its capacity to inhibit T cell activation and B cell proliferation, in addition to reinforcing the epithelial barrier. Although therapy in SS patients has generally consisted of systemic administration of immunosuppressive or antimuscarinic drugs, it has been known that the systemic use of these drugs induces severe side effects (34). In contrast, it has been reported that oral administration of rebamipide had no clinically significant physical side effects, with normal blood pressure and pulse rate, in healthy adult subjects (37). This study is the first to demonstrate that oral administration of rebamipide effectively inhibits autoimmune pathology in the NFS/*sld* mouse model of SS without causing systemic histopathologic changes.

We previously reported that a cleavage product of 120-kd α-fodrin may be an important autoantigen in the development of primary SS and that anti–120-kd α-fodrin antibodies have been frequently detected in sera from SS patients (25). We have also reported a significant increase in TUNEL+ apoptotic epithelial duct cells in the salivary glands of thymectomized NFS/*sld* mice and a large proportion of FasL in tissue-infiltrating CD4+ T cells (11); both findings support the idea that tissue-infiltrating CD4+ T cells are responsible for tissue destruction, as determined by in vitro cytotoxicity assay. Our data have suggested that one mechanism by which activated CD4+ T cells induce cytotoxicity to salivary gland cells in this murine model of SS is Fas-based and that the primary mediators of the disease are autoantigen-driven T cell responses. In the present study, we found that expression of FasL on CD4+ T cells was significantly inhibited and that TUNEL+ epithelial cell apoptosis declined in the rebamipide-treated mice. A significant decrease in autoantigen-specific T cell proliferation was observed in CD4+ T cells with rebamipide treatment. This is consistent with the finding that rebamipide treatment resulted in the dose-dependent inhibition of ovalbumin-specific T cell expansion in vivo.

In addition, we observed that rebamipide treatment induced a selective impairment of CD4+,CD62L^{low} effector T cells in the lymph nodes. This population was more potent than the population of CD4+,CD62L^{high} cells in inducing a self-directed immune response, as demonstrated by cytometric isolation and adoptive transfer experiments. The induction of autoimmunity by specific in vivo expansion of CD4+,CD62L^{low} cells has recently been demonstrated (29), indicating that CD4+,CD62L^{low} effector T cells may be attractive targets for immune interventions in the treatment of autoimmune diseases. On the other hand, rebamipide treatment did not influence the frequency of CD4+,CD25+ natural regulatory T cells in cervical lymph nodes (data not shown). It is noteworthy that rebamipide treatment inhibited T cell proliferation and Th1 cytokine production (IL-2 and IFNγ). These data indicate that rebamipide treatment effectively inhibits autoimmune pathology in the NFS/*sld* mouse model of SS.

The improvement in secretory function after treatment with rebamipide, as demonstrated by saliva volumes, strongly points to the ingestive mechanism of action of rebamipide. With regard to the small discrepancy between the histologic features of the lacrimal glands and the lacrimal gland function, as demonstrated by tear flow volumes after treatment of rebamipide (see Figure 1), it has been reported that inflammatory lesions in the lacrimal gland develop later than those in the salivary gland in our mouse model (22). It is also possible that the effects of rebamipide on salivary gland cells may be different from the effects on lacrimal gland cells.

The beneficial effects of rebamipide on the epithelial barrier, which have previously been demonstrated in the gastric and small intestinal mucosa (38,39), have possibly, although not definitively, also been shown for the salivary gland epithelia, although the findings are not definitive. While the mechanism of action of rebamipide

on epithelial permeability, which has mostly been studied in the stomach, is not completely understood, it could be related to the capacity of rebamipide to act as a scavenger of cytokine-induced hydroxyl radicals (40) or to induce prostaglandin production (41). Since we found decreased apoptosis of salivary gland epithelia in rebamipide-treated mice, it is possible that the protective effect of rebamipide on the salivary gland epithelia could also account for its beneficial effect on ulcerative colitis in humans or on Dextran sulfate sodium–induced colitis in rats (42). This improvement in the epithelial barrier, together with the capacity of rebamipide to modulate immune responses, may represent a new therapeutic approach to the clinical management of sicca syndrome in SS patients without producing any side effects.

Rebamipide treatment clearly inhibited the production of serum autoantibodies, IgM, and IgG1 and induced a reduction in the transcriptional activity of IRF-4 via down-regulation of NF-κB. It has been reported that IRF-4 functions redundantly with IRF-8 to regulate B cell differentiation into immature IgM+ B cells (43). IRF-4 has been shown to regulate the induction of BLIMP-1 expression and BLIMP-1–dependent plasma cell differentiation (44). The majority of IgM and IgG1 are autoreactive and are also reactive with DNA, phosphorylcholine, phosphatidylcholine, and α1–3-dextran. The process of autoantibody production in SS is characterized by findings of both an antigen-driven response and a polyclonal B cell activation. The causes of this abnormal activation have not been fully elucidated and are likely to vary in different patients and in different animal models of autoimmune diseases. These diseases are characterized by a high titer of autoantibodies that may play a role in the tissue damage. It is possible that the down-regulatory effect of rebamipide on the immune response would be a good therapeutic approach.

We have previously reported that treatment with anti-CD4 and anti-CD86 mAb, cathepsin S inhibitor, caspase inhibitor, and cyclosporin A improved the autoimmune pathology in this mouse model of SS (11,45–48). In the present study, we observed less drastic effects of rebamipide on histologic features, as compared with those in previous therapeutic experiments. This may be related to the relatively low degree of inhibitory effects on T cell–mediated immune responses. Although we did not simply compare the efficacy of rebamipide with that of systemic administration of a different agent, this successful therapeutic effect of rebamipide would provide the possibility of establishing a new form of therapy for patients with autoimmune symptoms caused by SS as well as other types of diseases.

ACKNOWLEDGMENTS

The authors thank Ai Nagaoka, Hiroyo Amo, and Satoko Yoshida for technical assistance.

AUTHOR CONTRIBUTIONS

Dr. Hayashi had full access to all of the data in the study and takes responsibility for the integrity of the data and the accuracy of the data analysis.

Study design. Kohashi, Ishimaru, Hayashi.
Acquisition of data. Kohashi, Arakaki.
Analysis and interpretation of data. Kohashi.
Manuscript preparation. Kohashi, Ishimaru, Hayashi.
Statistical analysis. Kohashi.

REFERENCES

1. Fox RI. Sjögren's syndrome. Lancet 2005;366:321–31.
2. Fox RI, Stern M, Michelson P. Update in Sjögren syndrome. Curr Opin Rheumatol 2000;12:391–8.
3. Kruize AA, Smeenk RJ, Kater L. Diagnostic criteria and immunopathogenesis of Sjögren's syndrome: implications for therapy. Immunol Today 1995;16:557–9.
4. Sebzda E, Mariathasan S, Ohteki T, Jones R, Bachmann MF, Ohashi PS. Selection of the T cell repertoire. Annu Rev Immunol 1999;17:829–74.
5. Starr TK, Jameson SC, Hogquist KA. Positive and negative selection of T cells. Annu Rev Immunol 2003;21:139–76.
6. Wakeland EK, Liu K, Graham RR, Behrens TW. Delineating the genetic basis of systemic lupus erythematosus. Immunity 2001;15:397–408.
7. Yasutomo K. Pathological lymphocyte activation by defective clearance of self-ligands in systemic lupus erythematosus. Rheumatology (Oxford) 2003;42:214–22.
8. Marrack P, Kappler J, Kotzin BL. Autoimmune disease: why and where it occurs. Nat Med 2001;7:899–905.
9. Davidson A, Diamond B. Autoimmune diseases. N Engl J Med 2001;345:340–50.
10. Yasutomo K, Horiuchi T, Kagami S, Tsukamoto H, Hashimura C, Urushihara M, et al. Mutation of DNASE1 in people with systemic lupus erythematosus. Nat Genet 2001;28:313–4.
11. Saegusa K, Ishimaru N, Yanagi K, Mishima K, Arakaki R, Suda T, et al. Prevention and induction of autoimmune exocrinopathy is dependent on pathogenic autoantigen cleavage in murine Sjögren's syndrome. J Immunol 2002;169:1050–7.
12. Bieganowska KD, Ausubel LJ, Modabber Y, Slovik E, Messersmith W, Hafler DA. Direct ex vivo analysis of activated, Fas-sensitive autoreactive T cells in human autoimmune disease. J Exp Med 1997;185:1585–94.
13. Miranda-Carus ME, Askanase AD, Clancy RM, Di Donato F, Chou TM, Libera MR, et al. Anti-SSA/Ro and anti-SSB/La autoantibodies bind the surface of apoptotic fetal cardiocytes and promote secretion of TNF-α by macrophages. J Immunol 2000;165:5345–51.
14. Avrameas S. Natural autoantibodies: from 'horror autotoxicus' to 'gnothi seauton'. Immunol Today 1991;12:154–9.
15. Toubi E, Etzioni A. Intravenous immunoglobulin in immunodeficiency states: state of the art. Clin Rev Allergy Immunol 2005;29:167–72.
16. Barabas AZ, Cole CD, Barabas AD, Lafreniere R. Production of

Immunity
Article

The Cytokine RANKL Produced by Positively Selected Thymocytes Fosters Medullary Thymic Epithelial Cells that Express Autoimmune Regulator

Yu Hikosaka,[1,10] Takeshi Nitta,[1,10] Izumi Ohigashi,[1] Kouta Yano,[1] Naozumi Ishimaru,[2] Yoshio Hayashi,[2] Mitsuru Matsumoto,[3] Koichi Matsuo,[4] Josef M. Penninger,[5] Hiroshi Takayanagi,[6] Yoshifumi Yokota,[7] Hisakata Yamada,[8] Yasunobu Yoshikai,[8] Jun-ichiro Inoue,[9] Taishin Akiyama,[9] and Yousuke Takahama[1,*]

[1]Division of Experimental Immunology, Institute for Genome Research
[2]Division of Oral Molecular Pathology, Institute of Health Biosciences
[3]Division of Molecular Immunology, Institute for Enzyme Research
University of Tokushima, Tokushima 770-8503, Japan
[4]Department of Microbiology and Immunology, School of Medicine, Keio University, Tokyo 160-8582, Japan
[5]Institute of Molecular Biotechnology, Austrian Academy of Science, 1030 Vienna, Austria
[6]Department of Cell Signaling, Tokyo Medical and Dental University, Tokyo 113-8549, Japan
[7]Division of Molecular Genetics, Faculty of Medical Sciences, University of Fukui, Fukui 910-1193, Japan
[8]Division of Host Defense, Medical Institute of Bioregulation, Kyushu University, Fukuoka 812-8582, Japan
[9]Division of Cellular and Molecular Biology, Institute of Medical Science, University of Tokyo, Tokyo 108-8639, Japan
[10]These authors contributed equally to this work
*Correspondence: takahama@genome.tokushima-u.ac.jp
DOI 10.1016/j.immuni.2008.06.018

SUMMARY

The thymic medulla provides a microenvironment where medullary thymic epithelial cells (mTECs) express autoimmune regulator and diverse tissue-restricted genes, contributing to launching self-tolerance. Positive selection is essential for thymic medulla formation via a previously unknown mechanism. Here we show that the cytokine RANK ligand (RANKL) was produced by positively selected thymocytes and regulated the cellularity of mTEC by interacting with RANK and osteoprotegerin. Forced expression of RANKL restored thymic medulla in mice lacking positive selection, whereas RANKL perturbation impaired medulla formation. These results indicate that RANKL produced by positively selected thymocytes is responsible for fostering thymic medulla formation, thereby establishing central tolerance.

INTRODUCTION

The thymus provides multiple microenvironments that sequentially support the development and selection of T lymphocytes. Thymocytes that express clonotypic and diverse T cell antigen receptors (TCR) are generated in the thymic cortex where cortical thymic epithelial cells (cTECs) present a set of self-peptides by virtue of proteasomes containing β5t and lysosomal proteases including cathepsin L (Finkel et al., 1989; Honey et al., 2002; Murata et al., 2007). TCR interaction with self-peptide-loaded MHC molecules expressed by cortical cells, including cTECs and hematopoietic cells, determines the life and death of immature thymocytes, and a fraction of cortical thymocytes survive TCR signals for further development (Kisielow et al., 1988; Daniels et al., 2006) and relocate to the thymic medulla chiefly via CCR7-mediated chemotaxis (Ueno et al., 2004; Kwan and Killeen, 2004). This process in the thymic cortex, referred to as positive selection, enriches T lymphocytes that demonstrate modest reactivity to self-peptides and potential responsiveness to foreign antigens. Entering the thymic medulla, positively selected semimature thymocytes further interact with self-peptides that are expressed by medullary thymic epithelial cells (mTECs) and dendritic cells (DCs). mTECs express a diverse set of genes representing essentially all tissues of the body, at least partly because of a nuclear molecule called autoimmune regulator (Aire) (Derbinski et al., 2001; Anderson et al., 2002), whereas thymic DCs, which efficiently present various self-peptides, are predominantly localized in the medulla and at least in part derived from circulation (Bonasio et al., 2006). The interaction of positively selected thymocytes in the thymic medulla with a diverse set of self-peptides, including tissue-restricted antigens presented by mTECs and DCs, is essential for establishing self-tolerance (Gallegos and Bevan, 2004).

Thymic medulla formation is dependent on the differentiation of mTECs from their endodermal precursor cells that are generated at the third pharyngeal pouch (Rossi et al., 2006; Bleul et al., 2006; Hamazaki et al., 2007), and the development of mTECs is regulated by the NF-κB activation pathway that includes transcription factor RelB and signal transducer TRAF6 (Burkly et al., 1995; Boehm et al., 2003; Akiyama et al., 2005). A recent study showed that $CD4^+CD3^-$ lymphoid tissue inducer (LTi) cells are involved in initiating embryonic mTEC development by producing the cytokine RANK ligand (RANKL) (Rossi et al., 2007).

Importantly, generation of the thymic microenvironment is also regulated by the development of thymocytes. This regulation is referred to as thymic crosstalk, and the signals produced by positively selected thymocytes are crucial for thymic medulla formation (Shores et al., 1991; van Ewijk et al., 1994). Mice deficient for the generation of mature thymocytes because of the lack of

positive selection exhibit defective medulla development (Philpott et al., 1992; Negishi et al., 1995), and reconstitution of the thymus with positively selected thymocytes restores formation of the medullary region (Surh et al., 1992; Nasreen et al., 2003). Thymus deficient for positive selection contains scattered and small clusters of mTECs, suggesting that positively selected thymocytes are responsible for the development of mTECs (Naspetti et al., 1997; Gray et al., 2006). Nonetheless, whether positive selection regulates the number or functional maturation of mTECs remains unclear. Molecular signals that regulate positive-selection-mediated medulla formation are also unknown.

The present study was aimed at identifying molecules that participate in positive-selection-mediated medulla formation in the thymus. We show that the interaction between RANKL produced by positively selected thymocytes and RANK and osteoprotegerin (OPG, a decoy receptor for RANKL) expressed by mTECs played a crucial role in positive-selection-mediated medulla formation by regulating the cellularity of Aire-expressing mTECs. We also present evidence that medulla formation in adult mice was chiefly regulated by positively selected thymocytes rather than by other intrathymic RANKL-expressing cells, including LTi cells. Thus, this study demonstrates that RANKL produced by positively selected thymocytes plays a major role in increasing the number of mTECs and forming thymic medulla that contains Aire-expressing mTECs.

RESULTS

Positive Selection Fosters Medulla Formation by Affecting mTEC Cellularity

It was previously shown that positive selection is crucial for thymic medulla formation and that mice lacking positive selection because of a deficiency of either TCRα or TCR-associated tyrosine kinase ZAP70 exhibit defective medulla formation in the thymus (Philpott et al., 1992; Negishi et al., 1995; also shown in hematoxylin-eosin-stained sections of Figure 1A). However, in agreement with previous findings (Naspetti et al., 1997; Gray et al., 2006), the scattered distribution of small mTEC clusters identified by mTEC-specific antibody ER-TR5 and mTEC-binding lectin UEA1 was detectable in the thymus of TCRα-deficient (*Tcra*$^{-/-}$) or ZAP70-deficient (*Zap70*$^{-/-}$) mice (Figure 1A). Flow cytometry analysis of thymic stromal cells showed that the numbers of mTEC identified as CD45$^-$I-A$^+$UEA1$^+$ or CD45$^-$I-A$^+$Ly51$^-$ were markedly reduced in TCRα-deficient or ZAP70-deficient mice (approximately 5%–10% of normal numbers), whereas the numbers of cTEC identified as CD45$^-$I-A$^+$UEA1$^-$ or CD45$^-$I-A$^+$Ly51$^+$ were not considerably reduced (Figures 1B and 1C). These results indicate that positive selection affects the number of mTECs but not of cTECs.

The major function of mTECs so far identified is to establish central tolerance by expressing a diverse set of tissue-restricted genes and by attracting positively selected cortical thymocytes for interaction with mTECs and DCs in the medulla (Derbinski et al., 2001; Anderson et al., 2002; Ueno et al., 2004; Kwan and Killeen, 2004; Gallegos and Bevan, 2004; Bonasio et al., 2006). Molecules involved in this mTEC function include Aire, a nuclear factor associated with promiscuous gene expression (Anderson et al., 2002), and CCL21, a chemokine that attracts positively selected thymocytes that express CCR7 (Ueno et al.,

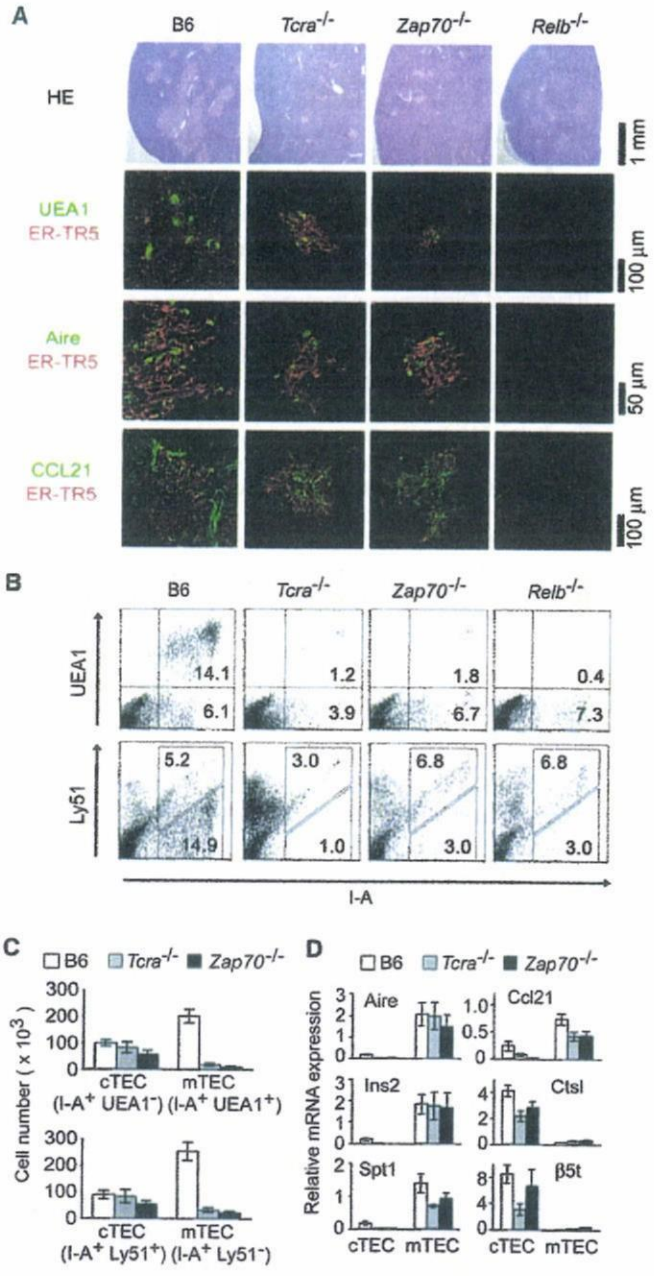

Figure 1. Positive Selection of Thymocytes Affects Number of mTECs

(A) Thymus lobes from 4- to 6-week-old young adult B6, *Tcra*$^{-/-}$, *Zap70*$^{-/-}$, or *Relb*$^{-/-}$ mice were stained with hematoxylin and eosin (HE) or with mTEC-specific monoclonal antibody ER-TR5 (red) and UEA1, antibody specific for Aire, or antibody specific for CCL21 (green).

(B) Two-color flow cytometry profiles for I-A and UEA1 (top) and I-A and Ly51 (bottom) of CD45$^-$ nonleukocytes prepared from thymuses of 4- to 6-week-old mice. Numbers indicate frequency of cells within indicated areas.

(C) Numbers of cTECs and mTECs per mouse in indicated mice. Averages and standard errors (B6, n = 4; *Tcra*$^{-/-}$, n = 4; *Zap70*$^{-/-}$, n = 3) are shown.

(D) Quantitative RT-PCR analysis of indicated genes in isolated cTECs and mTECs. mRNA expression was normalized to GAPDH mRNA, and those in CD45$^-$ total thymic stromal cells were arbitrarily set to 1. Averages and standard errors of at least three independent measurements are shown.

2004). Aire and CCL21 were detectable in mTEC clusters of TCRα-deficient or ZAP70-deficient mice, unlike in the thymus of RelB-deficient (*Relb*$^{-/-}$) mice where mTEC development was defective (Figure 1A). Quantitative mRNA analysis showed that mTECs isolated from TCRα-deficient or ZAP70-deficient mice indeed expressed Aire and CCL21 (Figure 1D). The generation of CD80-expressing mature mTECs was also detectable in TCRα-deficient or ZAP70-deficient mice (data not shown). The expression of Aire-dependent tissue-restricted genes, such as insulin 2 and salivary protein 1, was detectable in mTECs of TCRα-deficient or ZAP70-deficient mice, indicating that mTECs in these mice were capable of Aire-dependent promiscuous gene expression (Figure 1D). cTECs from TCRα-deficient or ZAP70-deficient mice expressed cathepsin L and β5t (Figure 1D), the molecules essential for thymocyte development in the cortex (Honey et al., 2002; Murata et al., 2007). These results indicate that mTECs and cTECs generated without positive selection express molecules that represent their functional maturity.

Small numbers of mTECs including Aire-expressing mTECs were detectable even in RAG2-deficient mice that lacked CD4$^+$CD8$^+$ (double-positive, DP) thymocytes (Derbinski et al., 2001; Rossi et al., 2007; also shown in Figure S1 available online), in agreement with the notion that functionally mature mTECs are generated without positive selection. Together, these results indicate that positive selection promotes the increase in the number of mTECs rather than the functional maturation of mTECs and thereby nurtures the formation of thymic medulla.

TNFSF Expressed in Thymocyte Subsets and TNFRSF Expressed in TEC Subsets

In order to explore the molecular mechanisms mediating the increase in mTEC cellularity caused by positive selection, we surveyed oligonucleotide microarray data from our previous study where we compared gene-expression profiles between positively selected TCR-transgenic thymocytes and wild-type thymocytes (Nitta et al., 2006). We noticed that genes encoding tumor necrosis factor superfamily (TNFSF) members, such as lymphotoxin (LT) α, LTβ, and RANKL, were strongly expressed in positively selected TCR-transgenic thymocytes (Table S1). We therefore analyzed the expression of all TNFSF genes in thymocyte subsets fractionated from normal adult thymus according to the expression of CD4 and CD8. As shown in Figure 2A and in agreement with microarray data, LTα, TNFα, LTβ, OX40L, CD40L, FasL, CD30L, and RANKL were expressed at significantly ($p < 0.05$) higher amounts in CD4$^+$CD8$^-$ and/or CD4$^-$CD8$^+$ (single-positive, SP) thymocytes than in DP thymocytes. LTα, TNFα, LTβ, CD30L, and RANKL expression was high in both CD4$^+$CD8$^-$ and CD4$^-$CD8$^+$ thymocytes, whereas OX40L, CD40L, and FasL expression was high in CD4$^+$CD8$^-$ thymocytes but not in CD4$^-$CD8$^+$ thymocytes. Other TNFSF members showed no significant difference ($p \geq 0.05$) in the expression between DP and SP thymocyte subsets.

We then analyzed the expression of TNF receptor superfamily (TNFRSF) genes in mTECs and cTECs isolated from normal adult thymus. We found that the genes for OX40, CD40, Fas, CD30, 4-1BB, TRAILR2, RANK, OPG, BAFFR, BCMA, RELT, and Eda2r were expressed at significantly ($p < 0.05$) higher amounts in mTECs than in cTECs (Figure 2B). In contrast, the expression of CD27, TWEAKR, GITR, and TNFRH3 was significantly ($p < 0.05$) higher in cTECs than in mTECs. Other TNFRSF members showed no significant difference ($p \geq 0.05$) in the expression between mTECs and cTECs.

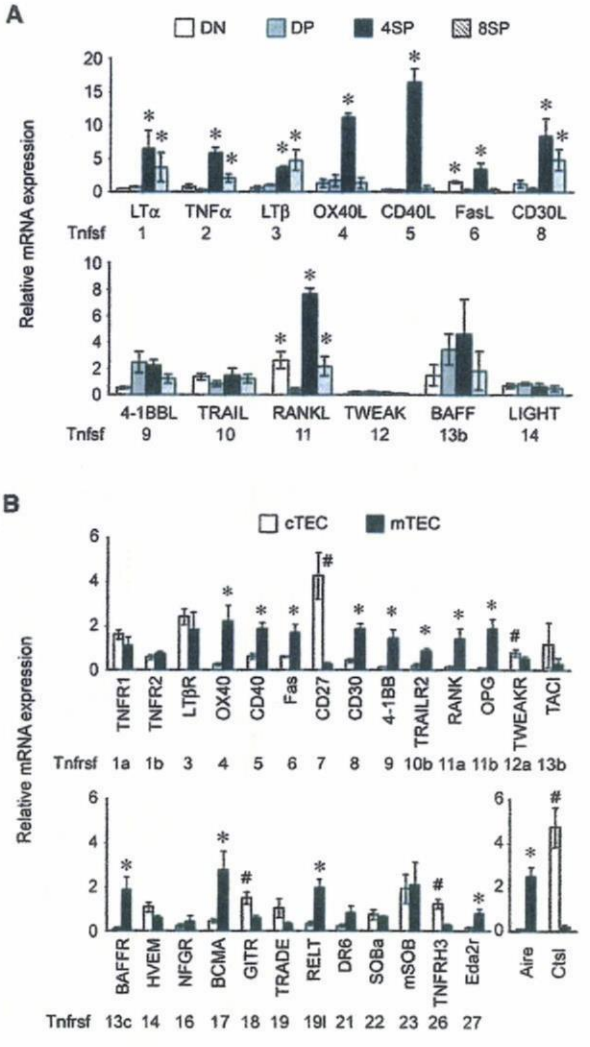

Figure 2. Expression of TNFSF Genes in Thymocytes and TNFRSF Genes in Thymic Epithelial Cells

(A) Quantitative RT-PCR analysis of sorted CD4$^-$CD8$^-$ (DN), CD4$^+$CD8$^+$ (DP), CD4$^+$CD8$^-$ (4SP), and CD4$^-$CD8$^+$ (8SP) thymocytes. mRNA expression of TNFSF genes was normalized to GAPDH mRNA, and those in total thymocytes were arbitrarily set to 1. Bar graphs show means ± standard errors of at least three independent measurements. Asterisks indicate significant ($p < 0.05$) increase compared to the amounts in DP thymocytes. mRNA expression of genes encoding Tnfsf7 (CD27L), Tnfsf13 (APRIL), Tnfsf15 (TL1), and Tnfsf18 (GITRL) was not detectable in total thymocytes or thymocyte subpopulations examined.

(B) Quantitative RT-PCR analysis of sorted CD45$^-$I-A$^+$UEA1$^-$ cTECs and CD45$^-$I-A$^+$UEA1$^+$ mTECs. mRNA expression of TNFRSF genes was normalized to GAPDH mRNA, and those in CD45$^-$ total thymic stromal cells were arbitrarily set to 1. Bar graphs show means ± standard errors of at least three independent measurements. Asterisks indicate significant ($p < 0.05$) increase in mRNAs in mTECs compared to those in cTECs, whereas sharps indicate significant ($p < 0.05$) increase in mRNA amounts in cTECs compared to those in mTECs. mRNA expression of Aire and cathepsin L (Ctsl) indicates successful isolation of mTECs and cTECs, respectively. mRNA expression of Tnfrsf25 (DR3) was not detectable in CD45$^-$ thymus cells, cTECs, or mTECs.

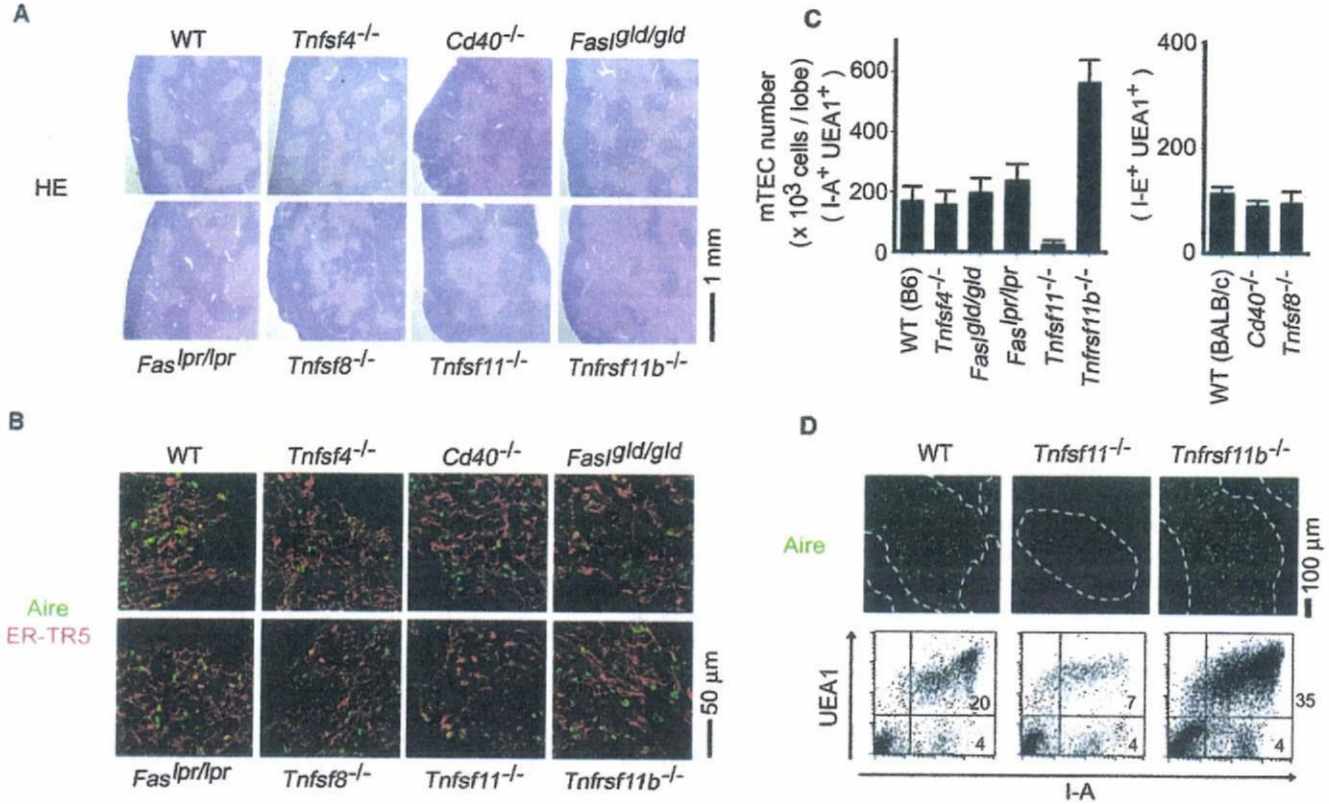

Figure 3. RANKL and OPG Affect Number of mTECs

(A and B) Thymus sections from indicated mice at 3–9 weeks old were analyzed by HE staining (A) and two-color immunostaining with antibody specific for Aire (green) and ER-TR5 (red) (B). B6 mice were used as wild-type (WT) control.

(C) Numbers of mTECs per thymus lobe were calculated by flow cytometry analysis of $CD45^-I\text{-}A^{b+}UEA1^+$ cells for mice of B6 background (left) and $CD45^-I\text{-}E^{d+}UEA1^+$ cells for mice of BALB/c background (right). Averages and standard errors are shown. B6, n = 6; *Tnfsf4*$^{-/-}$, n = 4; *Fasl*$^{gld/gld}$, n = 3; *Fas*$^{lpr/lpr}$, n = 3; *Tnfsf11*$^{-/-}$, n = 2; *Tnfrsf11b*$^{-/-}$, n = 3; BALB/c, n = 3; *Cd40*$^{-/-}$, n = 3; *Tnfsf8*$^{-/-}$, n = 3.

(D) Representative low-magnification images of Aire immunostaining in medullary region identified by ER-TR5 staining and marked by dotted lines, indicating that Aire-expressing cells are present in all three groups but are fewer and more detectable in the thymus of *Tnfsf11*$^{-/-}$ and *Tnfrsf11b*$^{-/-}$ mice, respectively, than in B6 wild-type (WT) mice. Representative two-color flow cytometry profiles for I-A and UEA1 of $CD45^-$ nonleukocytes of indicated mice are also shown. Numbers in quadrants indicate frequency of cells in boxes.

Consequently, we found that in the following five TNFSF ligand-receptor combinations, namely, between OX40L and OX40, between CD40L and CD40, between FasL and Fas, between CD30L and CD30, and among RANKL, RANK (signaling receptor for RANKL), and OPG (nonsignaling soluble decoy receptor for RANKL; Theill et al., 2002), ligands were more strongly expressed in SP thymocytes than in DP thymocytes and receptors were more strongly expressed in mTECs than in cTECs.

RANKL and OPG Influence mTEC Cellularity

We next examined mTEC development and medulla formation in mice deficient for one of the five TNFSF ligand-receptor combinations. We found that the deficiency of OX40L (*Tnfsf4*$^{-/-}$), CD40 (*Cd40*$^{-/-}$), FasL (*Fasl*$^{gld/gld}$), Fas (*Fas*$^{lpr/lpr}$), or CD30L (*Tnfsf8*$^{-/-}$) did not significantly ($p \geq 0.05$) affect the number of mTECs, the generation of Aire-expressing mTECs, or medulla formation (Figures 3A–3C). However, mice deficient for RANKL (*Tnfsf11*$^{-/-}$) exhibited a significant ($p < 0.05$) reduction in the number of mTECs (Figure 3C). In the thymus of RANKL-deficient mice, the number of Aire-expressing mTECs was also decreased as shown by immunohistological analysis (Figure 3D). Nonetheless, the development of Aire-expressing mTECs and the formation of thymic medulla were detectable in the thymus of RANKL-deficient mice (Figures 3A–3C). In contrast, mice deficient for OPG (*Tnfrsf11b*$^{-/-}$), a soluble decoy receptor for RANKL (Theill et al., 2002) and the receptor more strongly expressed in mTECs than in cTECs (Figure 2B), developed a significantly ($p < 0.05$) large number of mTECs and exhibited large thymic medulla with many Aire-expressing mTECs (Figures 3A–3D).

These results indicate that among TNFSF members that are more strongly expressed in SP thymocytes than in DP thymocytes, RANKL plays a major role in increasing the number of mTECs, and its decoy receptor, OPG, regulates mTEC cellularity and medulla formation.

RANKL Is Produced by Positively Selected Thymocytes

The expression of RANKL in normal adult mice was detectable in bulk $CD4^+CD8^-$ and $CD4^-CD8^+$ SP thymocytes but not DP thymocytes, as determined by quantitative mRNA analysis (Figures 2A and 4A). RANKL expression was detectable in $CD69^{hi}$ semimature and $CD69^{lo}$ mature $CD4^+CD8^-$ SP thymocytes isolated from normal B6 mice, both of which expressed $TCR\alpha\beta^{hi}$

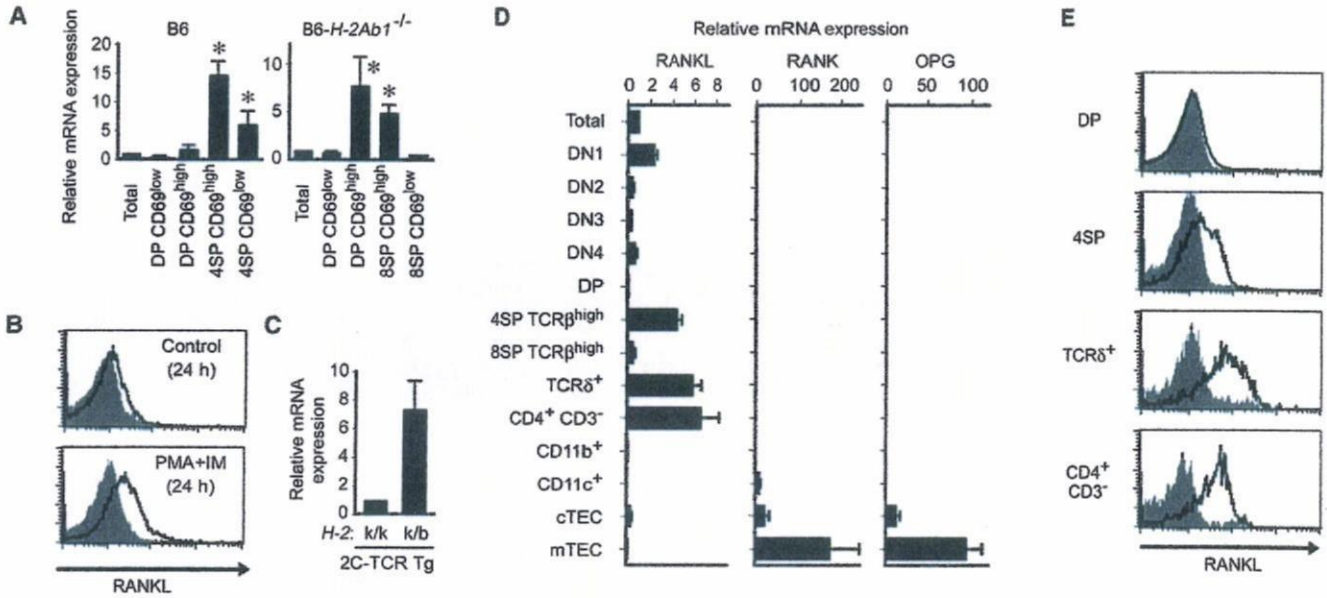

Figure 4. Expression of RANKL, RANK, and OPG in Thymus Cell Subpopulations

(A) mRNA expression of RANKL in total, $CD4^+CD8^+CD69^{lo}$, $CD4^+CD8^+CD69^{hi}$, $CD4^+CD8^-CD69^{hi}$, and $CD4^+CD8^-CD69^{lo}$ thymocytes isolated from 4-week-old B6 mice (n = 4), and total, $CD4^+CD8^+CD69^{lo}$, $CD4^+CD8^+CD69^{hi}$, $CD4^-CD8^+CD69^{hi}$, and $CD4^-CD8^+CD69^{lo}$ thymocytes isolated from MHC class II-deficient 4-week-old B6-*H-2Ab1*$^{-/-}$ mice (n = 3).

(B) Flow cytometry analysis of RANKL expression by TCR-stimulated thymocytes. Thymocytes from 3-week-old MHC class I and class II double-deficient B6-*H-2Ab1*$^{-/-}$*B2m*$^{-/-}$ mice were cultured in the absence or presence of phorbol 12-myristate 13-acetate (PMA, 0.2 ng/ml) and ionomycin (0.2 μg/ml) for 24 hr. RANKL staining profiles (solid lines) and control staining profiles (shaded lines) are shown. Representative profiles of three independent experiments are shown.

(C) mRNA expression of RANKL in $CD4^+CD8^+$ thymocytes isolated from positively selecting *H-2*$^{k/b}$ 2C-TCR-transgenic mice and null selecting *H-2*$^{k/k}$ 2C-TCR-transgenic mice (n = 3).

(D) mRNA expression of RANKL, RANK, and OPG in indicated thymus cell subpopulations isolated from 4- to 5-week-old B6 mice. DN1, DN2, DN3, and DN4 represent $CD4^-CD8^-CD25^-CD44^+$, $CD4^-CD8^-CD25^+CD44^+$, $CD4^-CD8^-CD25^+CD44^-$, and $CD4^-CD8^-CD25^-CD44^-$ thymocyte subpopulations. $CD4^+CD3^-CD8^-B220^-CD11c^-$ thymocyte subpopulation was used as $CD4^+CD3^-$ cells (Rossi et al., 2007). $CD45^-I\text{-}A^+UEA1^-$ cTECs and $CD45^-I\text{-}A^+UEA1^+$ mTECs were used. mRNA expression in total thymus cells are normalized to 1. Averages and standard errors (n = 3) are shown. Note that $CD4^+CD8^-TCR\beta^{hi}$ cells, $TCR\delta^+$ cells, and $CD4^+CD3^-$ cells are the three major cells that express RANKL mRNA in the thymus. RANKL expression detectable in DN1 ($CD44^+CD25^-CD4^-CD8^-$) cells may be due to $TCR\gamma\delta^+$ cells that are contained in DN1 population.

(E) Cell-surface RANKL detection (solid lines) and control staining (shaded lines) were examined in indicated subpopulations of 5-week-old B6 thymocytes incubated for 16 hr without stimulation. Representative profiles of three independent experiments are shown.

(Figure 4A). RANKL was also detectable in $CD69^{hi}$ semimature $CD4^-CD8^+$ SP thymocytes, rather than $CD69^{lo}$ mature $CD4^-CD8^+$ SP thymocytes, isolated from MHC class II-deficient mice (Figure 4A), indicating that RANKL is expressed in semimature thymocytes that are destined to become either $CD4^+CD8^-$ or $CD4^-CD8^+$ SP thymocytes. The $CD69^{hi}$ subpopulation of DP thymocytes, which represent semimature thymocytes that recently received positive-selection-inducing TCR signals (Bendelac et al., 1992), expressed a significantly ($p < 0.05$) higher amount of RANKL than the majority of DP thymocytes, which were $CD69^{lo}$, in MHC class II-deficient mice (Figure 4A). Stimulation of preselected DP thymocytes isolated from MHC class I- and MHC class II-deficient mice (*H-2Ab1*$^{-/-}$*B2m*$^{-/-}$) with plate-bound antibody specific for TCR or with phorbol ester plus ionomycin, which mimics positive-selection-inducing TCR signals (Takahama and Nakauchi, 1996), elevated cell-surface expression of RANKL protein (Figure 4B, data not shown). Indeed, DP thymocytes isolated from positively selecting 2C-TCR-transgenic mice expressed a significantly ($p < 0.05$) higher amount of RANKL than did DP thymocytes isolated from null selecting 2C-TCR-transgenic mice (Figure 4C). These results indicate that RANKL is produced in semimature thymocytes that recently received positive-selection-inducing TCR signals. These results also suggest that the amount and kinetics of RANKL expression may be unequal between cells destined to become $CD4^+CD8^-$ T lymphocytes and those destined to become $CD4^-CD8^+$ T lymphocytes.

TCRγδ$^+$ Cells or Id2-Dependent LTi Cells Are Dispensable for Medulla Formation in Adult Mice

To address whether cells other than positively selected thymocytes might produce RANKL in the thymus, we examined the expression of RANKL as well as its receptors, RANK and OPG, in various cell subpopulations isolated from adult thymus (Figure 4D). We found that in addition to positively selected SP thymocytes, RANKL expression in the thymus was highly detectable in $TCR\gamma\delta^+$ cells and $CD4^+CD3^-$ LTi cells, as assessed by quantitative mRNA analysis (Figure 4D) and by cell-surface protein analysis (Figure 4E). The detection of RANKL in SP thymocytes was specific, as indicated by the fact that no signals were detected in SP thymocytes isolated from RANKL-deficient mice (Figure S2). RANKL expression was detectable in CD4SP thymocytes from embryonic day 18.5 (E18.5) mice and 1-day-old newborn mice (Figure S3), suggesting that newly generated

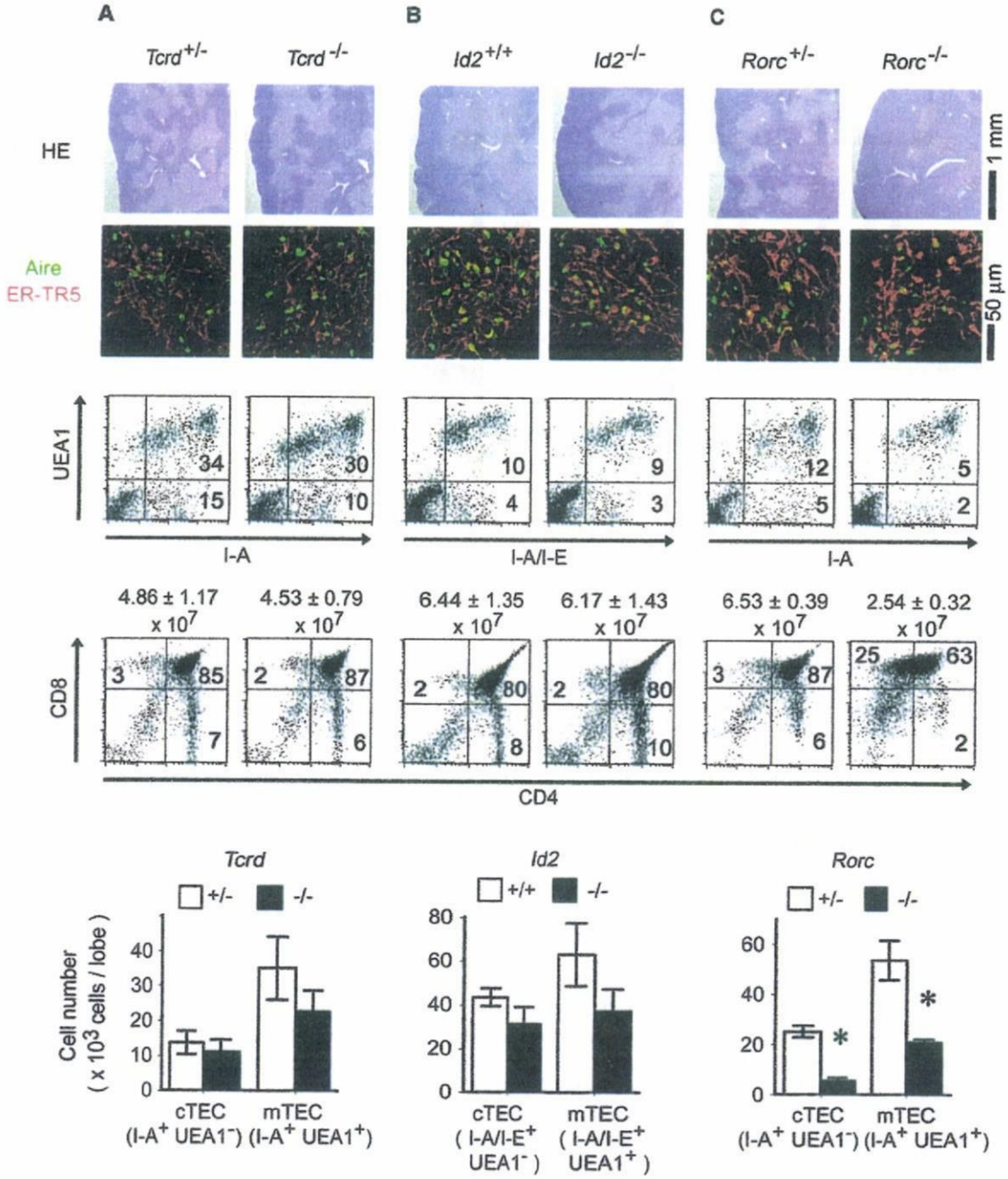

Figure 5. Thymic Epithelial Cells in TCRδ-, Id2-, or RORγt-Deficient Mice

Thymuses from age- and genetic background-matched *Tcrd*$^{+/-}$ and *Tcrd*$^{-/-}$ mice (B6 background [A]), *Id2*$^{+/+}$ and *Id2*$^{-/-}$ mice (ICR background [B]), or *Rorc*$^{+/-}$ and *Rorc*$^{-/-}$ mice (B6 background [C]) were subjected to section analysis and flow cytometry analysis as indicated. A monoclonal antibody specific for both I-A and I-E (clone M5/114) was used to detect class II MHC molecules in mice of ICR background. Averages and standard errors of thymocyte numbers per thymus lobe are also shown. Bar graphs show averages and standard errors of the numbers of CD45$^-$I-A$^+$UEA1$^-$ cTECs and CD45$^-$I-A$^+$UEA1$^+$ mTECs in indicated mice. *Tcrd*$^{+/-}$, n = 4; *Tcrd*$^{-/-}$, n = 5; *Id2*$^{+/+}$, n = 5; *Id2*$^{-/-}$, n = 6; *Rorc*$^{+/-}$, n = 3; *Rorc*$^{-/-}$, n = 3. Asterisks indicate significant difference ($p < 0.01$).

SP thymocytes can be the source of RANKL in the thymus. The detection of RANKL in CD4$^+$CD3$^-$ LTi cells of adult thymus was in agreement with previously reported results (Rossi et al., 2007). On the other hand, among thymic cell subpopulations examined, RANK and OPG were most prominently and almost exclusively detected in mTECs (Figure 4D).

In contrast to mice deficient for positive selection (Figure 1), we found no significant ($p \geq 0.05$) impairment in the number of mTECs or the development of thymic medulla containing Aire-expressing mTECs in adult mice lacking TCRδ (*Tcrd*$^{-/-}$) (Figure 5A) or adult mice deficient for Id2 (*Id2*$^{-/-}$) (Figure 5B; Figure S4), in which LTi cells in embryonic intestine are barely

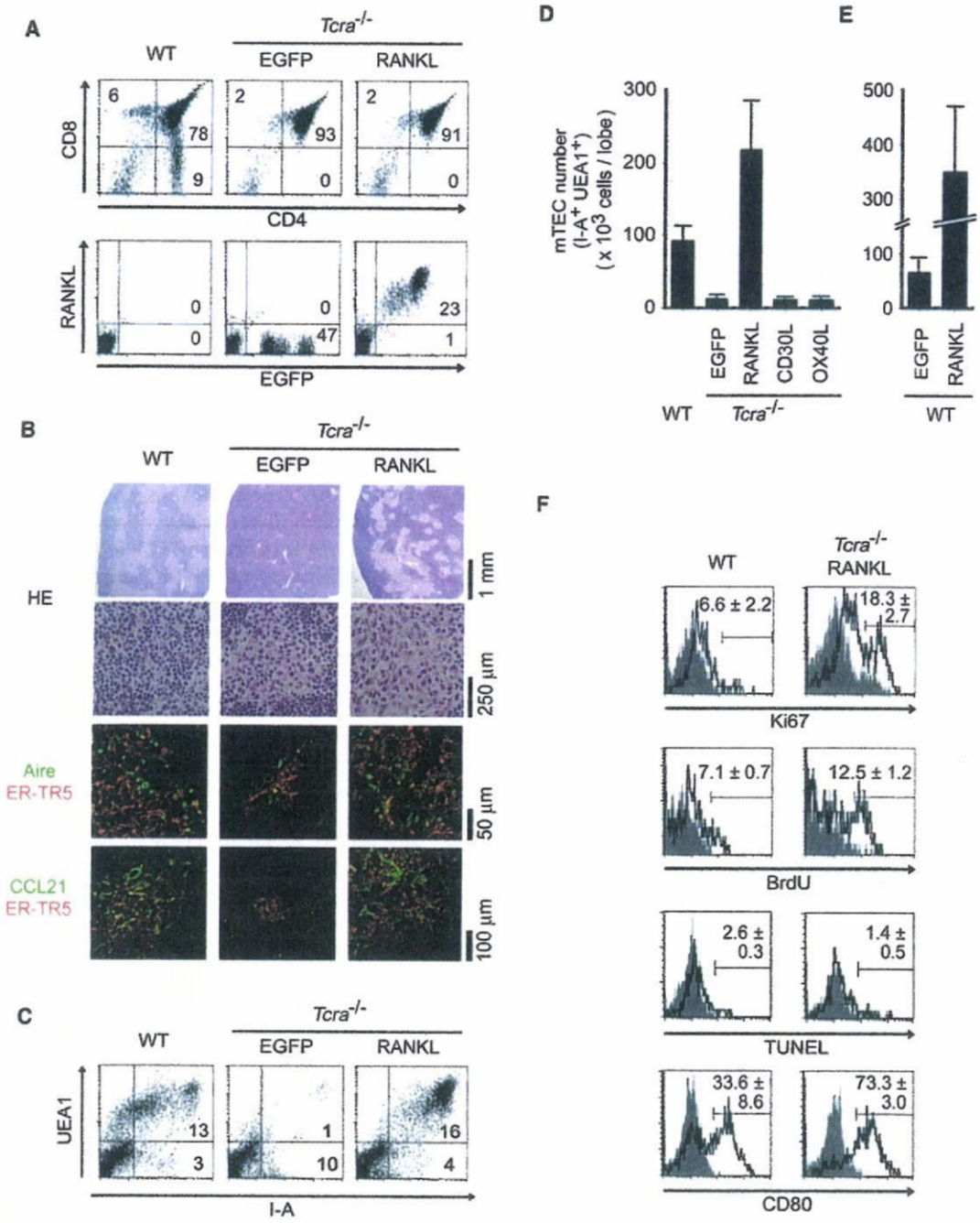

Figure 6. RANKL Expression Restores Medulla Formation without Positive Selection

Sca1+ bone marrow cells from *Tcra*$^{-/-}$ mice were infected with retrovirus expressing RANKL along with EGFP or EGFP alone, and transplanted into lethally irradiated *Tcra*$^{-/-}$ mice. Mice were analyzed 4–5 weeks after transplantation. Frequencies of EGFP+ cells in thymocytes ranged from 23% to 73%.

(A) Flow cytometry profiles of ungated thymocytes from adult B6 mice (WT), *Tcra*$^{-/-}$ mice expressing EGFP alone, or *Tcra*$^{-/-}$ mice expressing RANKL along with EGFP. Numbers indicate frequency of cells within indicated areas.

(B) Thymus section analysis. High-magnification HE-stained images show that thymic medullary areas generated in RANKL-expressing *Tcra*$^{-/-}$ mice are devoid of lymphoid cells, and this finding was supported by the failure to detect CD4- or CD8-expressing cells in those areas (not shown).

(C) Representative results of flow cytometry analysis for I-A+UEA1+ mTECs in CD45− nonleukocytes.

(D) Numbers (averages and standard errors) of CD45−I-A+UEA1+ mTECs per thymus lobe in B6 mice (WT) or *Tcra*$^{-/-}$ mice reconstituted with *Tcra*$^{-/-}$ bone marrow cells that retrovirally expressed EGFP alone or EGFP along with RANKL, CD30L, or OX40L. WT, n = 6; EGFP, n = 4; RANKL, n = 3; CD30L, n = 3; OX40L, n = 3.

(E) Numbers (averages and standard errors) of CD45−I-A+UEA1+ mTECs per thymus lobe in B6 mice (WT) reconstituted with bone marrow cells that expressed EGFP alone or EGFP along with RANKL, indicating that retroviral expression of RANKL increases the number of mTECs even in normal mice. EGFP, n = 4; RANKL, n = 3.

detectable (Yokota et al., 1999), indicating that unlike positively selected thymocytes, TCRγδ$^+$ cells and Id2-dependent LTi cells are dispensable for mTEC development and medulla formation in adult mice. However, the number of mTECs appeared slightly, although not significantly ($p \geq 0.05$), reduced in TCRδ-deficient mice or Id2-deficient mice (Figures 5A and 5B), suggesting that TCRγδ$^+$ cells and Id2-dependent LTi cells may partially contribute to the optimal cellularity of mTECs.

Similar to Id2-deficient mice, Aire-expressing mTECs were detectable in RORγt-deficient (*Rorc*$^{-/-}$) mice (Figure 5C) lacking LTi cells (Eberl et al., 2004). Unlike Id2-deficient mice, however, RORγt-deficient mice exhibited reduced number of mTECs and small medulla (Figure 5C). The deficiency in RORγt causes not only loss of LTi cells but also reduction in the numbers of DP and SP thymocytes because of reduced survival of DP thymocytes (Sun et al., 2000; also shown in Figure 5C). Accordingly, the number of cTECs was significantly ($p < 0.01$) reduced in RORγt-deficient mice, unlike Id2-deficient mice (Figures 5B and 5C). Thus, the reduced number of mTECs in RORγt-deficient mice may be due to the reduced number of DP and SP thymocytes, including positively selected thymocytes, rather than the loss of LTi cells.

RANKL Neutralization Perturbs mTEC Cellularity

The above-mentioned results suggest that RANKL produced by positively selected thymocytes plays a major role in expanding mTEC cellularity to form thymic medulla. We then examined whether RANKL expressed by developing thymocytes is essential for medulla formation in normal adult mice. To do so, normal B6 mice were reconstituted with B6 bone marrow hematopoietic progenitor cells that were infected with a retrovirus that expressed a soluble fusion protein of RANK and human immunoglobulin Fc portion (RANK-Fc) along with enhanced green fluorescence protein (EGFP). RANK-Fc fusion protein used in this study specifically binds to RANKL (Figure S5A) and neutralizes RANKL-mediated signals (Hsu et al., 1999). Thymocyte development, including the generation of SP thymocytes, was apparently not affected in RANK-Fc-expressing mice (Figure S5B). However, the number of mTECs was significantly ($p < 0.05$) reduced and thymic medulla containing Aire-expressing mTECs became underrepresented in B6 mice expressing RANK-Fc (Figures S5C–S5E). In contrast, RANK-Fc expression did not affect the number of cTECs (Figure S5E). These results indicate that in vivo blockade of RANKL perturbs mTEC cellularity and medulla formation in normal mice and that RANKL is essential for increasing mTEC cellularity and forming thymic medulla.

RANKL Expression Restores Thymic Medulla without Positive Selection

Finally, we addressed whether RANKL expression in developing thymocytes might be sufficient for increasing mTEC cellularity and forming thymic medulla even without positive selection. To do so, bone marrow hematopoietic progenitor cells from TCRα-deficient (*Tcra*$^{-/-}$) mice were infected with a retrovirus that expressed RANKL along with EGFP and were transferred into TCRα-deficient mice. In these mice, positive-selection-mediated generation of mature SP thymocytes remained defective because of the lack of TCR expression by DP thymocytes, whereas RANKL expression was detectable in the majority of EGFP$^+$ thymocytes (Figure 6A). We found that the number of mTECs was significantly ($p < 0.01$) restored and thymic medulla containing Aire-expressing and CCL21-expressing mTECs was obviously formed in RANKL-expressing TCRα-deficient mice but not in control EGFP-expressing TCRα-deficient mice (Figures 6B–6D). Thymic medulla formed in RANKL-expressing TCRα-deficient mice was not colonized with thymocytes because of the lack of positive selection (Figure 6B). Unlike RANKL expression, the expression of CD30L or OX40L did not restore the number of mTECs (Figure 6D). These results indicate that forced RANKL expression was sufficient in vivo for increasing mTEC cellularity and forming thymic medulla even without positive selection.

In order to better understand how RANKL expression increases mTEC cellularity, we measured Ki67 expression in proliferating cells, BrdU incorporation in DNA synthesizing cells, and TUNEL in dying cells, in mTECs of TCRα-deficient mice reconstituted with retrovirally RANKL-expressing TCRα-deficient bone marrow cells. As shown in Figure 6F, RANKL expression elevated the frequency of Ki67-expressing cells and BrdU-incorporated cells in mTECs compared to those in mTECs isolated from wild-type mice. The frequency of TUNEL$^+$ cells was only slightly reduced by RANKL expression (Figure 6F). RANKL expression also elevated the frequency of CD80-expressing mature cells in mTECs (Figure 6F). These results indicate that RANKL expression in bone-marrow-derived cells causes elevated proliferation of mTECs without positive selection, suggesting the possibility that RANKL contributes to medulla formation by promoting the proliferation of mTECs.

We finally addressed whether RANKL produced by SP thymocytes could directly promote the increase in mTEC cellularity. To do so, fetal thymus stromal cells were cultured with isolated SP thymocytes in reaggregated thymus organ culture. As shown in Figure 7, reaggregation with CD4SP thymocytes but not DP thymocytes significantly increased the number of mTECs but not cTECs in culture (Figures 7A and 7B). The number of CD80-expressing mature mTECs and the mRNA amounts of Aire and Aire-dependent tissue-restricted self-antigens (insulin 2 and salivary protein 1) were also increased by the addition of CD4SP thymocytes but not DP thymocytes (Figures 7B and 7C). Importantly, these increases in mTEC cellularity and the expression of mTEC-associated molecules were significantly ($p < 0.05$) diminished by the addition of RANK-Fc (Figure 7), which competitively antagonized RANKL (Figure S5). These results indicate that SP thymocytes are sufficient and RANKL is essential for fostering mTECs.

DISCUSSION

The present results show that positive selection promotes the increase in the number of mTECs and thereby fosters the

(F) Ki67 expression, BrdU incorporation, TUNEL, and CD80 expression were detected in CD45$^-$I-A$^+$UEA1$^+$ mTECs. BrdU (2 mg) was intravenously administered 24 hr before analysis. Shaded profiles indicate control staining. Numbers indicate averages and standard errors (from at least three independent measurements) of frequency of cells within indicated areas.